PLASMA NITRIDING BEHAVIOR OF AISI 5140 STEEL

A Thesis Submitted to the
Graduate School of Natural and Applied Sciences of
Dokuz Eylül University
In Partial Fulfillment of the Requirements for
the Doctor of Philosophy in Mechanical Engineering,
Material Sciences Program

by
Serdar KARAOĞLU

March, 1998
İZMİR

PLASMA NITRIDING BEHAVIOR OF AISI 5140 STEEL

by

Serdar KARAOĞLU

March, 1998

İZMİR

Ph.D. THESIS EXAMINATION RESULT FORM

We certify that we have read this thesis and that in our opinion it is fully adequate, in scope and in quality. As a thesis for the degree of Doctor of Philosophy.

Prof. Dr. Süleyman Karadeniz
(Advisor)

Prof. Dr. Kutsal Tülbentçi
(Committee Member)

Prof. Dr. Tevfik Aksoy
(Committee Member)

Approved for the
Graduate School of Natural and Applied Sciences

Prof.Dr.Cahit Helvacı
Director
Graduate School of Natural and Applied Sciences

ACKNOWLEDGEMENTS

I am gratefully acknowledge the support and encouragement given by Süleyman Karadeniz during the course of the investigation.

I am grateful to Faik Soysal for his helpful suggestions and assistance in carrying out the experiments. I am also grateful to Süleyman Güneş and Ahmet Yiğit for specimen preparation and other production work.

I am indebted to Seçil Erim and Ayhan Çelik for supplying valuable documents, and to Hatice Yılmaz for the SEM and XRD work.

During the thesis, assistance from these friends is also appreciated: E.Çınar Yeni, Zafer Azem, Hakan Aksakallı, İlkin İnci, Betül Akkuş, Nilay Karaoğlu, and Berk & Burhan Ayaşoğlu.

Finally, I thank my parents and my wife for their great help, encouragement and patience that supported me throughout the study.

Serdar KARAOĞLU

ABSTRACT

The plasma nitriding behavior of a low-alloy steel, AISI 5140, has been examined under various process conditions. The process variables studied include time (1-12h), temperature (450-550°C) and nitrogen partial pressure (10-60vol.%N_2) of nitriding atmosphere, which consisted of a mixture of N_2+H_2 with a total pressure of 10mbar. Microhardness measurements, optical microscopy, X-ray diffraction (XRD) and scanning electron microscopy (SEM) techniques have been utilized to investigate the nitriding response of the steel. The work has focused on the surface hardening behavior of the steel, the composition and morphology of the nitrided layers, and studies of fatigue and wear properties of plasma nitrided specimens. A reversed bending fatigue testing machine was used in fatigue tests. Wear tests were carried out under dry sliding conditions using a pin-on-ring configuration.

The maximum surface hardness was obtained in the sample plasma nitrided over a period of 4h at 500°C in a nitriding atmosphere containing 20vol.% N_2. For shorter treatment times and/or lower temperatures the amount of hardening was low due to the lower nitrogen uptake and precipitate density. Due to the coarser precipitates, extended nitriding periods and/or higher treatment temperatures led lower surface hardness as well.

XRD studies revealed that the outermost layer or compound layer of samples are made up of a mixture of γ′-nitride and ε-nitride phases. Formation of a predominantly γ′phase compound layer structure is favored at high temperatures, for long treatment times and by the use of low nitrogen atmospheres. The case depth and compound layer thickness were found to increase with increasing process temperature and time. Nitrogen content of the plasma nitriding atmosphere while increasing the compound layer thickness, slightly decreased the case depth.

The fatigue and wear tests revealed substantial improvements depending upon the structural characteristics of the component i.e. plasma nitriding process conditions. It was found that fatigue strength of a plasma nitrided sample was determined by its hardness and case depth. Fatigue fractography study using SEM revealed subsurface crack initiation especially on samples tested at low stress levels. Compound layer thickness, which seemed to have no significant effect on fatigue test results, played an important role in wear tests. Wear rates were observed to increase with increasing compound layer thickness and decreasing surface hardness.

ÖZET

Az alaşımlı bir çelik olan AISI 5140 ın plazma nitrürasyon davranışı çeşitli işlem şartları altında incelendi. İşlem değişkenleri olarak süre (1-12h), sıcaklık (450-550°C) ve N_2+H_2 karışımından oluşan plazma atmosferindeki azot gazının hacimsel oranı (%10-60) kullanıldı. Plazma nitrürasyon işlemleri 10mbar basınç altında gerçekleştirildi. Çeliğin nitrürasyon işlemine cevabını araştırmak için mikrosertlik ölçümü, optik mikroskobi, X-ışını difraksiyonu (XRD) ve taramalı elektron mikroskobi (SEM) teknikleri kullanıldı. Çalışma; çeliğin yüzey sertleşme davranışı, nitrürlenmiş tabakaların şekil ve kompozisyonu ile plazma nitrürlenmiş numunelerinin yorulma ve aşınma özelliklerinin araştırılmasında yoğunlaştı. Yorulma deneyleri eğilmeli tam değişken yükleme şartlarında, aşınma deneyleri ise pim-halka test düzeneğinde kuru sürtünme şartlarında gerçekleştirildi.

En yüksek yüzey sertliği; %20 N_2 içeren nitrürasyon ortamında, 500°C sıcaklıkta, 4 saat süreyle işlem gören numunelerde elde edildi. Daha alçak sıcaklıklarda ve/veya daha kısa işlemlerde, düşük azot girişi ve düşük çökelti yoğunluğu sebebiyle yüzey sertliğinin azaldığı görüldü. Uzun nitrürasyon sürelerinde ve/veya yüksek sıcaklıklarda ise çökeltilerin aşırı büyümesi ile sertlik azaldı.

XRD çalışmaları, numunelerin yüzeyindeki kompond tabakaların γ′ ve ε nitrür fazlarının bir karışımı olduğunu gösterdi. Yüksek sıcaklık, uzun işlem süresi ve düşük azot yüzdelerinin, γ′nitrürün yapıdaki ağırlığını arttırdığı tespit edildi. Difüzyon tabakası kalınlığı ile kompond tabaka kalınlığı artan işlem süresi ve sıcaklığı ile artmaktadır. Azot yüzdesinin artması ile kompond tabaka kalınlığında artma, difüzyon tabakası kalınlığında ise bir miktar azalma meydana gelmektedir.

Yorulma ve aşınma dayanımlarında, numunelerin yapısal karakteristiklerine dolayısı ile plazma nitrürasyon işlem şartlarına bağlı olarak işlem görmemiş parçalara göre önemli gelişmeler elde edilmiştir. Plazma nitrürlenmiş bir numunenin yorulma dayanımını, numunenin sertliği ve difüzyon tabakasının kalınlığı belirlemektedir. Taramalı elektron mikroskobu (SEM) ile yapılan yorulma kırıklarının incelenmesi sonunda, özellikle düşük gerilme seviyelerinde test edilen numunelerde yorulma çatlağının yüzeyin altından başladığı tespit edilmiştir. Yorulma dayanımına pek etki etmeyen kompond tabaka aşınma deneylerinde önemli bir rol oynamıştır. Aşınma miktarının, artan kompond tabaka kalınlığı ve azalan yüzey sertliği ile arttığı görülmüştür.

CONTENTS

Page

Contents VI
List of Tables VIII
List of Figures IX

Chapter One
INTRODUCTION

1.1 INTRODUCTION 1
1.2 LITERATURE REVIEW 2
1.3 AIM OF THE STUDY 7

Chapter Two
PLASMA NITRIDING

2.1 THE PRINCIPLE OF PLASMA NITRIDING 8
2.1.1 Equipment and Process Data 8
2.1.2 Technique and Control of the Glow Discharge 10
2.2 THE PLASMA STATE 11
2.2.1 Generation of the Plasma 11
2.2.2 The Reaction of the Plasma with the Surface of the Workpiece 13
2.3 THE DIFFUSION OF NITROGEN 16
2.4 STRUCTURE AND PROPERTIES OF PLASMA NITRIDED SURFACE LAYERS 18
2.4.1 The compound layer 20
2.4.2 The diffusion zone 23
2.5 THE ADVANTAGES OF PLASMA NITRIDING 25
2.6 INDUSTRIAL APPLICATIONS OF PLASMA NITRIDING 26
2.7 ECONOMIC CONSIDERATION 30

Page

Chapter Three
EXPERIMENTAL STUDIES

3.1 MATERIAL 32
3.2 PLASMA NITRIDING PROCEDURES 32
3.3 MICROHARDNESS TESTING AND OPTICAL MICROSCOPY 35
3.4 XRD AND SEM STUDIES 35
3.5 FATIGUE TESTING 36
3.6 WEAR TESTING 37

Chapter Four
RESULTS AND DISCUSSION

4.1 X-RAY DIFFRACTION ANALYSIS 39
4.2 MICROSTRUCTURE AND MICROHARDNESS 42
4.3 FATIGUE TESTS 51
4.3.1 S-N curves 51
4.3.2 Fractography 65
4.4 WEAR TESTS 71

Chapter Five
CONCLUSIONS

5.1 CONCLUSIONS 78

REFERENCES 81

APPENDIX 85

LIST OF TABLES

Page

Table 3.1 Chemical composition of test material (SAE 5140) 32
Table 3.2 Plasma nitriding process conditions 34
Table 4.1 Average values of microhardness, case depth and compound layer thickness of all specimen groups 44
Table 4.2 Fatigue test data of untreated specimen 53
Table 4.3 Fatigue test data of specimens plasma nitrided for 1 hour 54
Table 4.4 Fatigue test data of specimens plasma nitrided for 4 hours 55
Table 4.5 Fatigue test data of specimens plasma nitrided for 8 hours 56
Table 4.6 Fatigue test data of specimens plasma nitrided for 12 hours 57
Table 4.7 Fatigue test data of specimens plasma nitrided at 450°C 58
Table 4.8 Fatigue test data of specimens plasma nitrided at 550°C 59
Table 4.9 Fatigue test data of specimens plasma nitrided in atmospheres containing 10vol.%N_2 60
Table 4.10 Fatigue test data of specimens plasma nitrided in atmospheres containing 60vol.%N_2 61
Table 4.11 Average weight loss values of wear specimens 72

LIST OF FIGURES

Page

Figure 2.1. Plasma nitriding equipment 8
Figure 2.2. Voltage-current characteristics of different types of discharge 10
Figure 2.3. Workpieces surrounded by a glow seam 12
Figure 2.4. Surface reactions during plasma nitriding 14
Figure 2.5. Microstructure of plasma nitrided steel 19
Figure 2.6. Typical nitrogen and carbon concentration profiles of plasma nitrided steel 25
Figure 2.7 Typical load of 3500 gears made from AISI 4140 steel 28
Figure 2.8 Typical automotive components that are routinely plasma nitrided 29
Figure 3.1 Plasma-nitriding unit used in the investigations 33
Figure 3.2 The shape and dimensions of fatigue specimens 36
Figure 3.3 The fatigue testing machine 38
Figure 3.4 The wear testing machine 38
Figure 4.1 XRD patterns of specimens plasma nitrided for (a) 1h, (b) 4h, (c) 12h 40
Figure 4.2 Effect of process temperature and nitrogen concentration on the XRD patterns of specimens 41
Figure 4.3 XRD pattern of the sample 12.500.20 from the surface (a), and at a depth of approx. 5μm from the surface to the core (b) 42
Figure 4.4 Cross-sectional optical micrographs of plasma nitrided samples a)4.500.20 b)8.500.20 c)4.550.20 d)4.500.60 (etch 2% nital) 43
Figure 4.5 SEM micrograph of a sample treated at 450°C for 4h (4.450.20) 43
Figure 4.6 Microhardness-depth profiles of the specimens 45
Figure 4.7 Microhardness-depth profiles of samples plasma nitrided for 1, 4, 8, and 12h at 500°C 46

Page

Figure 4.8 a) Surface hardness b) Case depth and compound layer thickness as a function of plasma nitriding time 47
Figure 4.9 Microhardness-depth profiles of samples plasma nitrided at 450, 500, and 550°C for 4h 48
Figure 4.10 a) Surface hardness b) Case depth and compound layer thickness as a function of plasma nitriding temperature 48
Figure 4.11 Microhardness-depth profiles of samples plasma nitrided in atmospheres containing 10, 20, and 60 vol.% N2 at 500°C for 4h 50
Figure 4.12 a) Surface hardness b) Case depth and compound layer thickness as a function of N_2 content in plasma nitriding atmosphere 51
Figure 4.13 S-N curve for untreated specimens 53
Figure 4.14 S-N curve for specimen group 1.500.20 54
Figure 4.15 S-N curve for specimen group 4.500.20 55
Figure 4.16 S-N curve for specimen group 8.500.20 56
Figure 4.17 S-N curve for specimen group 12.500.20 57
Figure 4.18 S-N curve for specimen group 4.450.20 58
Figure 4.19 S-N curve for specimen group 4.550.20 59
Figure 4.20 S-N curve for specimen group 4.500.10 60
Figure 4.21 S-N curve for specimen group 4.500.60 61
Figure 4.22 S-N Curves of all the specimen groups 62
Figure 4.23 S-N curves of specimens plasma nitrided for 1, 4, 8, and 12h 62
Figure 4.24 S-N curves of specimens plasma nitrided at 450, 500, and 550°C 63
Figure 4.25 S-N curves of specimens plasma nitrided in various N_2 concentrations 63
Figure 4.26 Stress pattern in the tension side of a surface-hardened bar in bending 64
Figure 4.27 SEM fractographs of an untreated specimen with a life of 841600 cycles (Sample unt-17) a) Fatigue crack initiation area, b) well away the point of crack initiation (crack propagation area), c) final fracture region 66
Figure 4.28 SEM micrographs of some subsurface crack initiation areas 69

Page

Figure 4.29 Fracture origin of Sample 4.550.20-3 and its mating part showing particle-matrix decohesion and deformation at a subsurface non-metallic inclusion 70

Figure 4.30 SEM fractography showing typical fatigue striations at about 2,2 mm from the crack initiation area (Sample 1.500.20-19) 70

Figure 4.31 SEM fractographs of the typical fracture surface throughout the final fracture region showing dimple craters and inclusions 71

Figure 4.32 Wear curves for untreated and plasma nitrided samples 72

Figure 4.33 Scanning electron micrographs of worn surfaces of some specimens after a sliding distance of 400m a) untreated
b) Nitrided at 500°C for 4h (4.500.20)
c) Nitrided at 550 °C for 4h (4.550.20) 74

Figure 4.34 Scanning electron micrograph of a 4.550.20 sample showing the worn surface after a sliding distance of 1200m 75

Figure 4.35 Optical micrographs showing wear surfaces of a) untreated and b) plasma nitrided (4.500.20) samples after asliding distance of 2000m 75

Figure 4.36 Morphology of the wear debris particles produced from pins of a)untreated and b)plasma nitrided (4.500.20) samples 76

CHAPTER ONE
INTRODUCTION

1.1 INTRODUCTION

The surface of solid materials is subjected to interactions with the environment and sometimes is the location where the hardest requirements for the materials must be fulfilled.

It is well known that the structure, composition and properties of the surface determine many operational characteristics of machine components. Surfaces of metal parts can be made hard and wear resistant by means of a variety of surface treatments. Among the thermochemical processes for the improvement of surface properties of machine components, nitriding has a great importance in industry today.

Together with conventional gas and bath nitriding there is a new process called plasma nitriding or ion-nitriding which has become available to the production engineer with the advent of glow discharge plasma surface engineering. Plasma nitriding, a completely environmentally harmless technology, has been developed to complete industrial application in the last few decades. Today, plasma nitriding is used on a large scale in industries concerned with iron, steel, cast iron, titanium and sintered iron products.

Because of its special basic technique -making use of the plasma of a glow discharge- plasma nitriding has a large variety of properties to offer and therefore opens up new perspectives in the field of nitriding.

The great number of treatment parameters which can be arbitrarily selected and precisely preset within wide limits, make it possible to produce specific structures and properties not

found in normal nitrided steels. For this reason plasma nitriding is in many cases superior to the conventional nitriding processes.

Plasma nitriding is carried out in a nitrogen-hydrogen gas mixture at 1 to 10 Torr pressure. Under the influence of a high dc voltage the gas is ionized and becomes electrically conductive. Positive gas ions are attracted by the cathodic workpieces where, on hitting their surface, they cause the nitriding action. The outer layers formed on metal components by the inward diffusion of nitrogen consist of two layers which are clearly distinguishable on metallographic examination. The compound layer at the surface is rich in nitrogen and only a few micrometers in thickness. This is supported by the significantly thicker diffusion layer. In diffusion layer the nitrogen is present in solute form or as special nitride compounds. On the other hand, the compound layer consists of an intermetallic compound of iron plus nitrogen (γ' and ε).

1.2 LITERATURE REVIEW

The concept and principles of the plasma nitriding process were first established in Germany by Bernard Berghaus in the early 1930's (Berghaus,1932). The following work was concerned with the establishment and control of glow discharges from high currents (Berghaus,1939; Berghaus,1956; Berghaus,1961).

Ionen, a private company owned by Berghaus in Cologne-Germany was responsible for the industrial exploitation of the technology generated. Following the death of Berghaus in 1965, Klockner Ionen was formed in 1967 and thus gained access to this technology which formed the basis of the international commercialization of this technique (Hombeck & Bell,1991). Plasma nitriding installations of various sizes have been available from the Klockner Ionen GmbH, Cologne, Germany since 1972 (Edenhofer,1976). Today, industrial installations operate in many countries, and heat treatment corporations having plasma nitriding units can be visited in Internet web sites.

The results of studies on the physical aspects or mechanism of the process are quite conflicting. No consensus has been reached about a proper model of the process so far (Li

& Manory, 1996). The Kölbel (Kölbel, 1965) and Hudis (Hudis, 1973) models in particular are very well known, but the mechanism of nitriding described in each of them is totally different. In Kölbel's model elemental iron is sputtered from the cathode workpiece by nitrogen ions and highly energized neutral particles. These iron atoms form FeN in the plasma which is deposited on the workpiece surface. Since FeN is not a thermally stable compound, it degrades to iron nitrides with a lower nitrogen content, producing nitrogen atoms that are capable of diffusion. The continuous diffusion of the nitrogen atoms into the material's surface forms the required case. Based on mass spectrometry results, Hudis (Hudis, 1973) suggests that nitrogen mass transfer during plasma nitriding is predominantly due to bombardment of the workpiece by plasma species containing nitrogen. Another study on the mechanism of the process (Tibbets,1974) pointed out the adsorption of neutral atomic nitrogen to be the cause of nitriding.

Normally, specimens in plasma nitriding process are in cathode position and they are heated to the process temperature by the ion bombardment. But in the case of samples at the anode position radiation heating (Zlatonovic, Kunosic & Tomcik, 1986), or resistance heating (Michalski, 1993) can be applied. In the former study, Zlatonovic et al. explained the process by the direct diffusion of the active species from the cathode to the anode. In the other investigation, Michalski studied Armco iron plasma nitrided in various glow discharge regions, i.e. on the cathode, on the anode, and on a substrate isolated from the cathode and anode (at plasma potential). He saw that the nitriding process would occur in regions other than the cathodic region if the substrate is hot enough. He examined the differences in the growth kinetics and surface morphology of the nitrided layers, depending on the region where nitriding process took place. It has been concluded that, sputtering effect is not necessary for glow discharge nitriding and atomic nitrogen can be chemisorbed on the hot surface and diffuse deep into the substrate.

After the first laboratory experiments and patents, many plasma nitriding studies have been conducted primarily dealing with the metallurgical aspects, i.e. the influence of the plasma nitriding treatment on the different materials, the production of different layers and the examination of their properties.

In their Transmission Electron Microscopy (TEM) study, Phillips and Seybolt (Phillips & Seybolt, 1968) investigated some plasma nitrided binary iron alloys and steels. They observed particle formation where hardening occurred. They have characterized the large nitride particles (7-60 nm wide by 25-60 nm in apparent thickness) but the finely (about 1nm in diam.) dispersed "dots" which are believed to be the cause of the surface hardening, have been impossible to characterize even after 1 h anneals at 650°C to induce coarsening of the particles. They also concluded that the maximum surface hardness was approximately inversely proportional to the nitride particle size. In order to observe the individual role of the alloying elements in steels Seybolt (Seybolt, 1969) examined the plasma nitrided eight binary alloys with respect to the microstructure, hardness level, and depth. He reported that among Al, Mo, Mn, Si, Ti, V, Cr, and C, only Al, Cr, Ti, and V additions caused hardening in binary iron alloys. In these studies, N_2/H_2 ratio was kept approximately 2% to minimize the formation of compound layer so as to examine the alloy nitrides in the diffusion zone.

İnal and Robino (İnal & Robino, 1982; Robino & İnal, 1983) researched the structures of plasma nitrided low alloy commercial steels using field ion microscopy (FIM) and transmission electron microscopy (TEM) techniques, and the relationship between nitriding parameters and hardenability characteristics of the steels. These studies showed that, the nucleation and growth of very small nitride precipitates adjacent to the carbides were already present following tempering. This was seen as an indication of the dissolution of the carbides during the process, although some of the carbides were still undissolved following 10h of plasma nitriding at 520°C.

The outermost layer, compound layer or white layer, of the plasma nitrided materials has been the subject of many studies. Investigations related to structure, composition and thickness of the compound layer have been carried out using X-ray diffraction (XRD), Transmission Electron Microscopy (TEM), Electron Probe Micro Analysis (EPMA), Optical Microscopy and Scanning Electron Microscopy (SEM) techniques.

Kurny, Mallya and Mohan Rao (Kurny, Mallya & Mohan Rao, 1986) investigated the nature of the compound layer formed on a plasma nitrided low alloy steel (En40B) by the XRD technique and optical metallography. They reported that the structure of the compound layer gradually transforms from a predominantly ε nitride to a predominantly γ′

nitride structure with increasing treatment time. They also observed that the thickness of the compound layer produced after about 5h of treatment, decreases with further increase in time.

Chyou and Shih (Chyou & Shih, 1990) investigated the structure and electrochemical properties of a plasma nitrided low alloy steel (AISI 4140). They observed that γ' forms at greater depths than ε.

Based on a TEM study (Xu, Wang, Yu & Hei, 1996) it was concluded that; the compound layer consists of columnar ε and γ', the former precipitating thin γ' phases in some orientations, and supersaturating nitrogen atoms produces lattice distortion in the columnar γ'.

Çelik and Karadeniz (Çelik & Karadeniz, 1996) investigated the structure and composition of compound layer formed on a low alloy steel (AISI 4140) plasma nitrided at various process conditions. They observed a decrease in the thickness of the compound layer at higher treatment temperatures and longer treatment times.

Recently, some investigations (Haruman, Bell & Sun, 1992; Lampe, Eisenberg & Laudien, 1993; Li & Manory, 1996) on the phenomenon of pore formation on the top surface of compound layer have appeared.

Plasma nitriding has been gradually incorporated in many industrial applications particularly during the last 25 years. Workers in plasma nitriding have explored the possibilities of this technique almost in every type of steel. Besides studies on low alloy steels, some examples of which given above, there have been many investigations concerning plasma nitriding behavior of high alloy steels (Cohen, Boas & Rosen, 1986; Özbaysal, İnal & Romig, 1986; Takada, Ohizumi, Miyamura, Kuwahara, Kikuchi & Tamura, 1986; Miyamura, Takada, Kuwahara & Kikuchi, 1986; Sato, Takahashi, Inoue, Yamazaki & Nitoh, 1988; Albarran, Juarez-Islas & Martinez, 1992; Kuppasami, Terrance, Sundararaman & Raghunathan, 1993; Kuppasami, Sundararaman & Raghunathan, 1993).

Studies related to fatigue properties of plasma nitrided materials are quite rare. It has been generally demonstrated by fatigue testing that it was the nitrided case (diffusion zone) which had a dominating effect on the fatigue behavior of plasma nitrided specimens and compound layer thickness had no influence on the fatigue limit (Sun & Bell, 1991). This behavior can be explained by the fatigue fracture mechanism of plasma nitrided specimens. It was observed by several investigators (Jones & Martin, 1978; Çelik & Karadeniz, 1995) that fatigue cracks originated from non-metallic inclusions at the case-core transition zone i.e. subsurface cracking occurred. It is envisaged, therefore, that a compound layer on the surface has no dominating influence on the initiation and propagation of fatigue cracks and increasing the nitrided case depth increases the fatigue limit of the steel (Sun & Bell, 1991).

The wear mechanism of plasma nitriding steels is not fully understood, even though it has been extensively studied.

Bell and Sun (Bell & Sun, 1990) showed that a thick and strong nitrided case is required for plasma nitrided specimens to bear high loads without severe wear. In another study (Karamış,1991) on the same low alloy steel (En40B) with similar process conditions a combination of higher hardness and deeper case has been advised for reducing the extent of material lost under dry and abrasive-containing lubricated conditions. It was surprisingly observed that some samples having a thicker compound layer wear less than others under dry conditions.

It has been experimentally demonstrated by e.g. Sun and Bell (Sun & Bell, 1991), and Karamış (Karamış,1992; Karamış, 1993) that a poly-phased and thick compound layer, which is extremely brittle, increases the wear rate of the materials especially at the initial stage of the wear process. But this is not a general rule and there are several examples (e.g. Karamış,1991) of contradicting behavior.

Peng (Peng, 1989) investigated the abrasive wear behavior of a hot work die steel subjected to a range of surface treatments such as nitrocarburising, plasma nitriding and spark discharge cladding. He concluded that modified surfaces possess improved resistance to abrasive wear, and plasma nitrided surfaces has the highest relative wear resistance.

The wear behavior of plasma nitrided martensitic stainless steel, AISI 440C, has been investigated under various contact conditions (Sun, Bell & Wood, 1994) and it was observed that the short time nitrided layers exhibited better wear resistance than the long time nitrided layers produced at similar temperatures.

1.3 AIM OF THE STUDY

The aim of this study is to investigate the plasma nitriding behavior of a low-alloy steel, AISI 5140 (DIN 41Cr4). Most of the work has focused on; the surface hardening behavior of the steel, the composition and morphology of the nitrided layers, and studies of fatigue and wear properties of plasma nitrided specimens.

For this purpose, first, specimens were plasma nitrided for various parameters such as time, temperature, and gas composition. Then, thickness and composition of compound layer were examined using optical metallography and X-ray diffraction (XRD) technique respectively. After that, microhardness measurements were utilized to obtain the hardness profiles of plasma nitrided samples. Finally, fatigue and wear tests were carried out to determine the effect of plasma nitriding process on the performance of the specimens. Based on the analysis of the results, correlation between process parameters and mechanical properties of the specimens were examined.

CHAPTER TWO
PLASMA NITRIDING

2.1 THE PRINCIPLE OF PLASMA NITRIDING

2.1.1 Equipment and Process Data

In order to get a better understanding of the glow discharge technique used in plasma nitriding and of the processes involved, we must first consider the plasma nitriding equipment (Fig.2.1). Its main elements are the vacuum furnace, the gas distribution system and the electric unit.

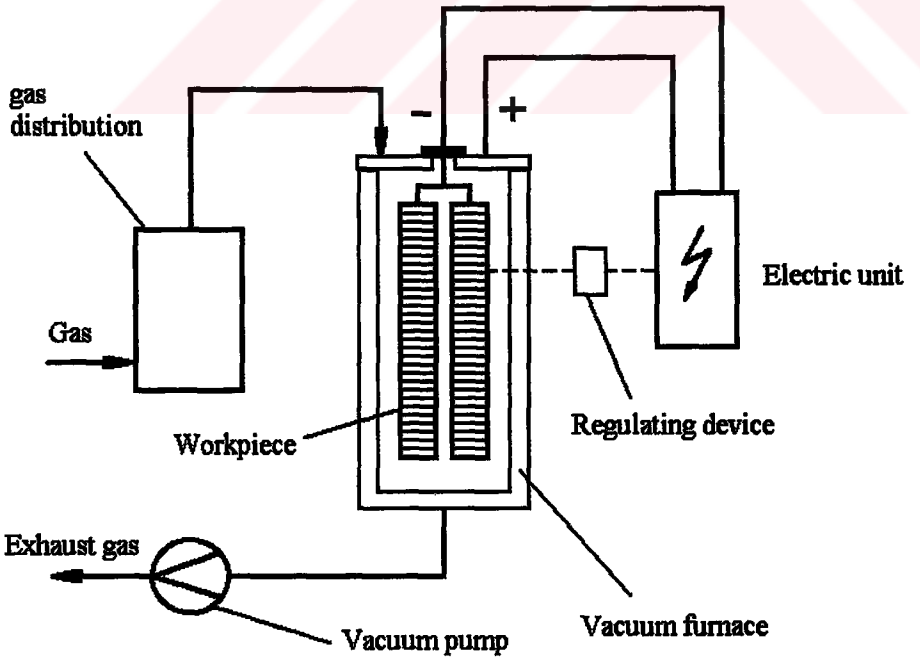

Figure 2.1 Plasma nitriding equipment

The components to be plasma nitrided are electrically isolated and suspended or placed in the vacuum furnace. Together with the vacuum pump, the gas distribution system enables the furnace to be evacuated, filled with the appropriate treatment gas and maintained at the required vacuum, usually between 13.3 to1333 Pa (0.1 to 10 torr). A d.c. voltage which can be set any value from about 100 volts to approximately 1500 volts, is applied between the cathode on which the workpiece to be plasma nitrided is placed and the anode which is usually connected to the wall of the furnace. Under this potential difference, the molecules and atoms of the treatment gas are excited and ionized, producing the typical luminous phenomenon known as glow discharge. The positive ions of the treatment gas are accelerated towards the negatively connected component and hit its surface with tremendous kinetic energy. The release of this energy heats the workpiece up and the ions are occluded into its surface. Thus, the furnace does not require a separate heating system.

Plasma nitriding can be carried out using either pure nitrogen or mixtures of nitrogen with hydrogen. Gas consumption during processing is very modest due to the low pressure employed.

The electric units are equipped with current and voltage control elements as well as a high speed breaker system to control unstable discharge phenomena.

The temperature of the workpiece is measured with the aid of thermocouples and regulated by means of a controller varying the power output of the electric unit. The treatment temperature is, in most cases, set between 400 and 600 °C , depending on the composition and structure of the material to be treated as well as the stress which the workpiece will have to resist. A particular advantage of plasma nitriding is the fact that even at low temperatures of between 350 and 450 °C nitrogen saturation of the surface is possible.

Typical treatment times vary from 1 hour to 20 hours, depending on the grade of steel and the required depth of hardening. But some investigations employing treatment times as long as 100 hours have appeared in the literature (Karamış,1991; Karamış, 1992; Karamış, 1993; Sun, Bell & Wood, 1994)

2.1.2 Technique and Control of the Glow Discharge

A glow discharge is produced by the shock excitation of gas atoms and molecules in an electric field in accordance with physical laws. The prerequisites of the appearance of a glow discharge are the presence of a low pressure gas (medium-high vacuum) and the application of a voltage of about 300 V minimum depending upon the gas pressure between two electrodes in the discharge vessel. Fig.2.2 shows the voltage-current characteristics of different types of discharge. The regions A-B (range of the Geiger-counter tube), B-C (Townsend discharge), etc., where the current is extremely low, are of no interest here. The normal glow discharges used in industry (glow lamps, fluorescent tubes, etc.) are maintained with relatively low energies and weak currents, i.e. they work in the region of normal stable and low current glow discharge (E-F). Plasma nitriding processes, however, are associated with high current and power densities and occur in the region of the abnormal, unstable and current-intensive glow discharge. The command and control of this unstable, abnormal glow discharge is the most essential feature in the production of truly plasma nitrided surface layers. The characteristics of this type of discharge clearly indicate that quite a few problems are involved in such control. When working in this abnormal region of the glow discharge (just in front of point G) a slight, localized increase in current density would quickly result in a concentration of the discharge at that particular point.

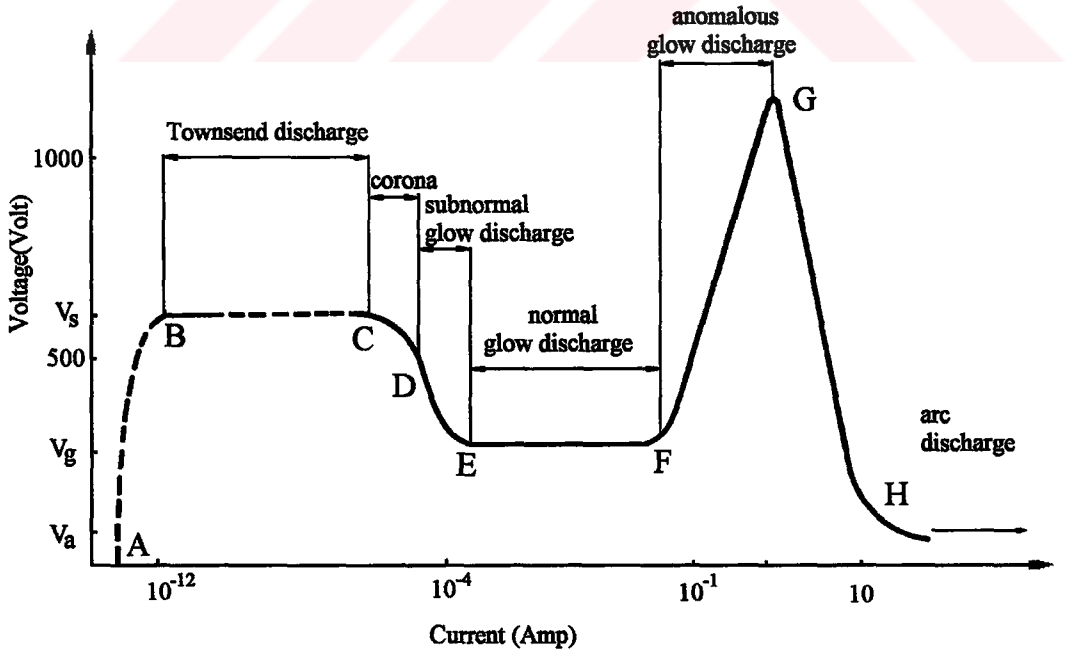

Figure 2.2 Voltage-current characteristics of different types of discharge

The possibility that the abnormal, unstable glow discharge may turn into the stable arc discharge has long been a serious obstacle to the large-scale application of plasma nitriding in industry. It was a major achievement of Bernhard Berghaus to realize these problems at an early stage and to have solved them subsequently by systematic developments (Edenhofer, 1974a).

Nowadays, modern electronic high-speed breaker systems are able to interrogate the current and voltage variations about a thousand times per second and interrupt the discharge for very short periods even if only slight changes are detected. These systems prevent the formation of arcs so that the glow discharge can be safely maintained at high current densities in the extremely abnormal region.

2.2 THE PLASMA STATE

A variety of nitrogen-providing media are used in nitriding. In accordance with the well known states of matter, nitriding may be classified as solid nitriding, liquid nitriding or gas nitriding. In addition to these three states of matter, there is a further, much more active condition sometimes described as fourth state of matter: the plasma state. As the name infers "plasma nitriding" uses this plasma state.

2.2.1 Generation of the plasma

A plasma consists of electrically charged particles, i.e. ions and electrons. In other words, the plasma state is reached by ionizing gas atoms or molecules. In a purely thermal process, this state can only be reached by heating gas to a temperature of at least some hundred thousand degrees. If, however, electricity is employed, this state can be easily reached as in the glow discharge. The small number of charge carriers which are present in any gas are accelerated in the voltage drop between cathode and anode. Collision processes involving other gas particles will dissociate molecules of the treatment gas as well as excite and ionize atoms and molecules. New charge carriers are thus continuously produced; the electrons being accelerated towards the anodically-connected wall of the furnace and the positive ions towards the cathodically-connected workpiece.

The possibility that the abnormal, unstable glow discharge may turn into the stable arc discharge has long been a serious obstacle to the large-scale application of plasma nitriding in industry. It was a major achievement of Bernhard Berghaus to realize these problems at an early stage and to have solved them subsequently by systematic developments (Edenhofer, 1974a).

Nowadays, modern electronic high-speed breaker systems are able to interrogate the current and voltage variations about a thousand times per second and interrupt the discharge for very short periods even if only slight changes are detected. These systems prevent the formation of arcs so that the glow discharge can be safely maintained at high current densities in the extremely abnormal region.

2.2 THE PLASMA STATE

A variety of nitrogen-providing media are used in nitriding. In accordance with the well known states of matter, nitriding may be classified as solid nitriding, liquid nitriding or gas nitriding. In addition to these three states of matter, there is a further, much more active condition sometimes described as fourth state of matter: the plasma state. As the name infers "plasma nitriding" uses this plasma state.

2.2.1 Generation of the plasma

A plasma consists of electrically charged particles, i.e. ions and electrons. In other words, the plasma state is reached by ionizing gas atoms or molecules. In a purely thermal process, this state can only be reached by heating gas to a temperature of at least some hundred thousand degrees. If, however, electricity is employed, this state can be easily reached as in the glow discharge. The small number of charge carriers which are present in any gas are accelerated in the voltage drop between cathode and anode. Collision processes involving other gas particles will dissociate molecules of the treatment gas as well as excite and ionize atoms and molecules. New charge carriers are thus continuously produced; the electrons being accelerated towards the anodically-connected wall of the furnace and the positive ions towards the cathodically-connected workpiece.

The voltage applied does not drop in a linear way between the wall of the furnace and the workpiece, such as it would in an extremely high vacuum, but is greatly modified by the positive space charge which builds up in front of the workpiece. Accordingly, almost the entire applied voltage drops only a few millimeters in front of the cathode (see the upper part of Fig.2.4). This is why the voltage drop is called "cathode fall". All the collision and ionization processes which are an essential feature of this type of surface treatment take place within the region of the cathode fall. Thus, the perfect plasma state of the treatment gas is only produced immediately in front of the workpiece surface (within the cathode fall region), while the remaining treatment space in the vacuum furnace is filled with normal treatment gas which is somewhat enriched in charge carriers. The positive space charge has the effect of a projecting anode so that surface treatment in the plasma of the glow discharge is practically independent of the distance between the workpiece and the wall of the furnace.

The cathodic luminous phenomena called "glow seam" is also limited to a narrow space around the workpiece as can be seen in Fig.2.3. This figure shows the interior of the plasma nitriding vacuum chamber, used in this study, charged with various workpieces. The glow seam follows each individual contour of the workpieces so that all surfaces, including notches and bores, are submitted to uniform ion bombardment, creating a uniform hardness.

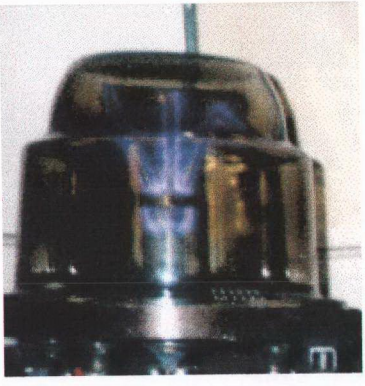

Figure 2.3 Workpieces surrounded by a glow seam

2.2.2 The reaction of the plasma with the surface of the workpiece

In the cathode fall, the positive nitrogen ions produced by collision processes are strongly accelerated towards the surface of the workpiece. Depending on the voltage applied and the number of particles available, kinetic energies ranging from a few, to several hundred electron volts are produced in this process. These values correspond to atomic plasma temperatures of about ten thousand to several hundred thousand degrees.

After having traversed the applied voltage, these "hot" i.e. high-energy, ions hit the workpiece surface with a certain kinetic energy (E_{ion}). This may give rise to the following processes:

1) Sputtering

When the ions hit the surface of the workpiece, metal atoms (Fe as well as alloy constituents such as Cr, Mo, Al, W, etc.) are detached (Fig.2.4). Sputtering may be considered a vaporization process the very "hot" ion hitting the surface will intensely heat a localized surface area of the workpiece causing atoms in that particular region to vaporize. These localized temperatures of several thousand degrees are limited to extremely small surface areas and do not harm the workpiece. The average temperature of the surface corresponds exactly to the workpiece temperature, as it was preset, in accordance with the required treatment. This can be proved by measuring the temperatures with the aid of thermocouples or radiation pyrometers.

During this sputtering process, part of the ion energy is converted into work (A) to detach atoms and electrons from the surface, and into kinetic energy (E_{kin}) of the detached particles.

$$E_{ion} = A + E_{kin}$$

As well as metals, non metallic elements such as carbon, oxygen, nitrogen, etc. are also detached (Fig.2.4). In this way the surface can be freed from carbides, oxides, etc. Due to the secondary diffusion of these elements (preferably along the grain boundaries) to the surface, the sputtering process has a profound effect upon their concentration and behavior even inside the material.

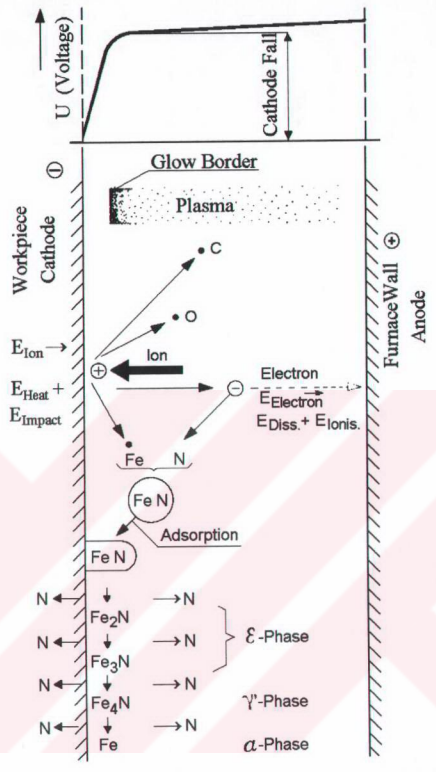

Figure 2.4 Surface reactions during plasma nitriding

As far as oxygen is concerned, sputtering results in a unique surface depassivation. This applies also to the strongly adherent oxide layers found on high chromium and stainless steels.

2) Heating

When the nitrogen ions hit and penetrate the topmost atom layers of the workpiece surface, the remaining ion energy is converted into heat (Q) to heat the workpiece. Thus the workpieces to be treated do not require any external heating. The following equation of the energy balance results:

$$E_{ion} \Rightarrow A + E_{kin} + Q$$

If gas mixtures are used instead of pure nitrogen, ions of other elements such as hydrogen, carbon, oxygen, etc. will also be able to penetrate and heat the workpiece.

3) Condensation

It is only to an extremely small extent that the transfer of nitrogen from the plasma into the surface of the workpiece is caused by direct occlusion of ions into the iron lattice (ion bombardment). The most important factor dominating the nitrogen absorption is associated with the sputtering process referred to above. Iron atoms which are detached from the surface can combine with the highly reactive nitrogen atoms in the plasma near the surface of the workpiece and will then, owing to adsorption, be deposited as iron nitride (FeN) on the workpiece surface (Kölbel, 1965). Thus an appositely directed condensation process is superimposed on the sputtering effect.

The iron nitride (FeN) produced in the plasma, having a theoretical nitrogen content of 25.05 per cent by weight, can be condensed on a constantly-cooled surface where, with suitably intensive cooling, the majority of it can be preserved. Investigations of such condensation processes have indicated that the nitride FeN is actually produced during plasma nitriding. Up to 19.7% of nitrogen could be found by chemical analysis of the condensate. The FeN nitride which is condensed on uncooled cathodic workpiece surfaces (i.e. 400 to 600 °C depending on the plasma nitriding temperature) is unstable and decomposes into the lower nitrides Fe_2N, Fe_3N, and Fe_4N (Fig.2.4) (Kölbel, 1965). The nitrogen which is liberated in this process will diffuse into the workpiece and, in part , back into the plasma.

The two processes sputtering and condensation, depend to a great extent on the type of gas used (ammonia, nitrogen, hydrocarbon, etc.). Furthermore, their mutual relationship can be influenced by varying other treatment parameters such as the pressure and voltage.

If for example, the gas pressure is set to a lower value (reduced particle density), there are longer free paths with a smaller probability collision. The detached atoms can thus move

a greater distance away from the workpiece surface, i.e. the possibility of back-diffusion is reduced. Such a parameter setting is of importance in depassivation processes in connection with the removal of oxide layers.

If the gas pressure in the furnace is higher, there is increased back-diffusion. The gas pressure setting can therefore be used to control the thickness of the compound zone.

The material transfer and the resulting increase or decrease in the weight of the workpiece is mainly controlled by the two counteracting processes of sputtering and condensation. Positive and negative changes in weight as well as extremely precise dimensional control can thus be obtained by varying the intensity of these two processes.

2.3 THE DIFFUSION OF NITROGEN

Investigations into the kinetics of nitriding have been made since the introduction of the process and continue today. In particular, attempts have been made again and again to reduce the extremely long treatment times associated with conventional gas nitriding by accelerating the process of nitrogen occlusion. The first laboratory tests of the plasma nitriding process showed that, as compared to gas nitriding, plasma nitriding considerably reduced the time of nitrogen occlusion.

Although this accelerated hardening effect in plasma nitriding has not been of primary importance in the large scale industrial application of the process, the decisive factors being the precisely controllable structure of plasma nitrided components and their resulting special properties, it is important, from a metallurgical point of view, to know which factors cause the accelerated nitrogen diffusion.

The explanation given in previous years - depassivation of the surface due to cathode sputtering and increased gas activity - were bound to remain inconclusive as long as the kinetics of the formation of plasma nitrided layers were unknown.

It was not until the nitrogen occlusion in plasma nitriding was found to be mainly caused by the iron sputtering and the subsequent iron nitride (FeN) condensation on the surface

(Kölbel, 1965), that a reasonable explanation of the accelerated diffusion in plasma nitriding could be given.

Thus at the very outset of the plasma nitriding process, the nitrogen-rich phase (FeN) is condensed on the workpiece surface -its immediate disintegration liberates nitrogen which diffuses into the workpiece. In gas nitriding, the surface concentration of nitrogen is established gradually, first a solid solution in ferrite (α-iron) and then conversion to nitrides with increasing nitrogen content- Fe_4N, $Fe_{3-2}N$. The abundant supply of nitrogen in plasma nitriding results in a very fast nitrogen saturation of the α-iron so that, only a few minutes later, coherent layers of iron nitrides exist in equilibrium with the saturated iron. For precisely the same reason, plasma nitriding at extremely low temperatures e.g. 350°C, can produce compact coherent iron nitride layers after only a few hours.

The FeN iron nitride which is condensed on the surface and the resulting high surface concentration of nitrogen yield a concentration gradient which is very steep at the beginning. Experimental results show that it is only after treatment times of ten hours and more that the nitrogen penetration in plasma nitriding no longer progresses at a faster rate in gas nitriding.

On the basis of these results it becomes obvious that the increased concentration gradient alone cannot account for the accelerated diffusion observed. With the build-up of coherent iron nitride phases in gas nitriding, (after about 1 to 2 hours) the concentration gradients in the two processes become similar, since the saturation concentration of the α-iron is reached.

The other important factor with regard to the depth of nitrogen penetration, the temperature dependent rate of diffusion of nitrogen in iron, can be positively influenced by plasma nitriding. It was experimentally demonstrated that the diffusion of nitrogen in the first stage of the gas nitriding process occurs mainly along the grain boundaries. This is understandable, considering that the catalytic disassociation of the ammonia gas on the surface of the steel would occur preferably, in areas of high energy. In intercrystalline diffusion, the nitrogen contacts the carbide phases in the grain boundaries. Due to the

occlusion of nitrogen in the carbides, these begin to grow considerably and are, at the same time, converted into carbonitrides. This effect involves quite a waste of nitrogen and badly interferes with the grain boundary diffusion. For this reason the transcrystalline diffusion of nitrogen in gas nitriding (characterized by the formation of finely dispersed nitrides in the α) is retarded.

On the other hand, most of the nitrogen is found to undergone transcrystalline diffusion right from the beginning of the process in plasma nitriding. This effect is due to the even condensation of the iron nitride from the plasma on the entire surface of the workpiece allowing a plane diffusion front to enter the whole material. Furthermore, the controllable partial sputtering of the carbon from the surface and the after-diffusion of carbon, mainly along the grain boundaries, cause something like decarburisation of the grain boundaries in the area close to the surface , so that those nitrogen atoms which diffuse along the grain boundaries cannot form any carbonitride phases which would inhibit further diffusion. An additional significant effect of the prevention of carbonitride precipitation in the grain boundaries close to the surface (up to 100 μm) lies in the considerable decrease in the brittleness of the nitride-hardened surface layers.

The two essential factors of the accelerated diffusion of nitrogen in plasma nitriding are the high surface concentration of nitrogen, which is of particular significance at the beginning of the process, and the increased rate of nitrogen penetration due to the different diffusion mechanism.

2.4 STRUCTURE AND PROPERTIES OF PLASMA NITRIDED SURFACE LAYERS

After plasma nitriding, the surface layers have essentially the same macroscopic structure as conventionally nitrided surfaces. There are, however, considerable differences with regard to microscopic details. The structure and possible layer modifications described below apply to plasma nitrided ferrous materials with a maximum of 10% of metallic alloying elements.

Fig.2.5 shows the typical microstructure of plasma nitrided steel. The outermost layer, which is very thin and consists mainly of iron nitrides, is not attacked by an alcoholic nitric acid etch so that it is white on the micrograph. For this reason, the layer is usually referred to as "white layer". With regard to the structure and the special character of this layer, the more recent term "compound layer" is, however, more to the point. Beneath the compound layer is the so-called diffusion zone where the nitrogen has mainly been incorporated into the existing iron lattice as interstitial atoms or as a finely dispersed alloy nitride precipitate. The thickness of the diffusion zone depends on the temperature, time of treatment and the alloy content of the steel.

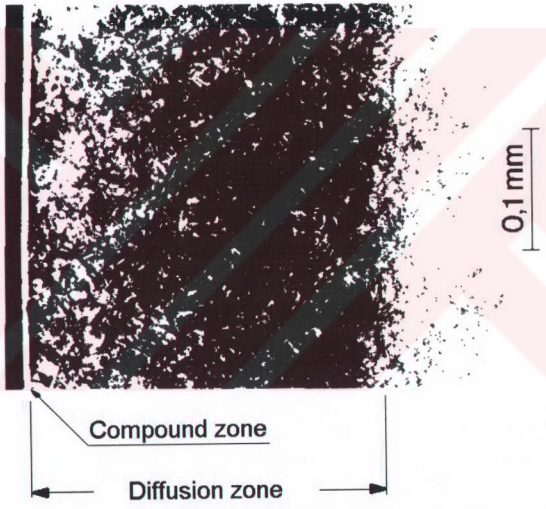

Figure 2.5 Microstructure of plasma nitrided steel

In contrast to conventional nitriding processes where, practically, only the thickness of these two zones can be varied within close limits, plasma nitriding offers the possibility of effecting several, precisely controllable, modifications to them, yielding very special properties. This ability to vary their structure is due to the great number of adjustable treatment parameters. The alteration of such parameters as voltage, current, gas pressure, gas composition, temperature, etc. has a direct influence on the fundamental physical phenomena of plasma nitriding. The different structure of plasma nitrided surface layers are

usually achieved by means of the sputtering rate, which can be controlled by varying the voltage, or the pressure and composition of the gas mixture.

The properties of a plasma nitrided steel component are determined by both the core strength and the structural characteristics of the compound layer and the diffusion zone.

2.4.1 The Compound Layer

It is well recognized that for each fixed process condition there exist a critical nitrogen potential, called the threshold nitriding potential, below which an iron nitride layer does not form on the surface during plasma nitriding (Sun & Bell, 1991). In other words, reduction of the amount of available nitrogen at the surface during the process leads to complete suppression of compound layer formation (Lampe et al, 1993; Kovacs & Russell, 1986). Nitriding without iron nitride layer formation is usually called "bright nitriding".

By varying nitriding potential (i.e. N_2:H_2 ratio) for various times, threshold nitriding potential curves can be obtained experimentally for a given process temperature. The time required to obtain an iron nitride layer increases with decreasing nitriding potential. The time dependence of the threshold nitriding potential is in agreement with the fact that there exists an incubation time for the formation of the iron nitride layer. Indeed, during nitriding, the surface nitrogen concentration is built up gradually with time and the incubation time for the formation of the iron nitride layer is obviously the time necessary for the built up of the critical nitrogen concentration on the surface. Obviously, the threshold nitriding potential curve is temperature dependent. In the case of conventional gas nitriding it was observed that the curve moves upwards with increasing temperature, whilst in plasma nitriding the opposite trend was observed. This could be explained by the different nitriding and mass transfer mechanisms occurring in the gaseous and plasma processes (Sun & Bell, 1991).

When the nitriding potential (N_2:H_2 ratio) is above the threshold value, a compound layer consisting of γ' (Fe_4N) and/or ε ($Fe_{2\text{-}3}N$) will form on the surface of a steel component. It was experimentally demonstrated that even in carbon-free nitrogenous plasma a poly-phase ($\gamma'+\varepsilon$) compound layer was usually produced on the surface of low alloy steel. A monophase γ' iron nitride layer can be produced only when the nitriding temperature is very

high or the nitriding potential is sufficiently low. With decreasing nitriding temperature and time or increasing nitriding potential the relative amount of ε phase formed in the compound layer is increased. The carbon content in the steel has a significant influence on the phase composition of the compound layer. The ε:γ′ ratio in the compound layer increases with increasing carbon content in the substrate (Sun & Bell, 1991; Karamış, 1992). Similarly, the introduction of carbon-containing gases into the nitriding atmosphere (plasma nitrocarburising) results in a compound layer composed of mainly ε phase. By careful control of the carbon content in the plasma, it is possible to produce a monophase ε iron nitride layer which has superior resistance to seizure and scuffing (Edenhofer, 1974b; Sun & Bell, 1991).

The development of the iron nitride layer is determined by nitriding temperature and time as well as nitriding potential. Decreasing the nitriding potential in the nitriding atmosphere, leads to a considerable reduction in the thickness of the iron nitride layer. Therefore, an iron nitride layer of high quality and desired thickness can be readily produced by monitoring the flow rate of N_2 and H_2 to the chamber. However, the development of the iron nitride layer only approximated to a parabolic dependence on time for the first few hours of nitriding, until a limiting thickness is reached, beyond which no further growth is observed (Sun & Bell, 1991; Karamış, 1992; Edenhofer, 1974b). It is believed that cathode sputtering plays an important role in determining the growth of the compound layer. By controlling the rate of sputtering, the thickness of the compound layer can be preset to the optimum, i.e. the minimum value that enables the workpiece to cope with the anticipated working conditions (Edenhofer, 1974b).

Investigations related to structure and mechanical properties of plasma nitrided steels have shown that the usefulness of the compound layer depends mainly on two factors: the homogeneity of the nitride structure and the thickness of the layer. With regard to the homogeneity of the nitride structure, the mechanical properties were found to be considerably better if the compound layer consisted of only one nitride phase, i.e. either γ′ or ε nitride. In poly-phased compound layers, containing a heterogeneous mixture of γ′ and ε phases, there are high inherent stresses in the transitional region between the different lattice structures (γ′: face centered cubic and ε: hexagonal) which may give rise to micro-

cracks if even a slight external stress is superimposed. The brittleness of the compound layer produced by gas nitriding (always poly-phased γ′ plus ε) and the less brittle compound layer of bath nitrided workpieces (exclusively ε nitride) confirm the influence of layer homogeneity.

As far as the thickness of the nitride structure is concerned, it is well known that the ductility of the layer decreases with increasing layer thickness.

Based on these two factors, the optimum properties will be produced when the compound layer is mono-phased (practical experience showed that small amount of mixed phases are of secondary importance) and of the minimum thickness necessary to meet specific property requirements such as wear and corrosion resistance. Careful control of the plasma nitriding process enables these two conditions to be met quite easily (Edenhofer, 1974b).

The carbon content in the steel also has a significant influence on the development of the compound layer. Under the same plasma process conditions the compound layer thickness increases with increasing carbon content in the substrate. Increasing the carbon content in steel increases the amount of ε phase in the compound layer, thus giving rise to the growth rate of the layer (Sun & Bell, 1991; Karamış, 1992).

Although the absence of porosity was shown by Edenhofer (Edenhofer, 1974b) as an advantage of the plasma nitriding, Lampe et.al. (Lampe et.al., 1993) pointed out that during plasma nitriding fine pores can form in the grain boundary zones of the compound layer. However, no pore channels with a direct link to the surface (as occur with salt bath nitriding) were observed. They also observed that the pores were formed in both types of nitrides and the quantity and size of individual pores increased with length of treatment and in particular at higher processing temperatures.

Extremely high levels of porosity, as can sometimes occur with salt bath nitriding and which are desirable under certain circumstances for specific applications, can not be

achieved by plasma nitriding, since the nitrogen content of the compound layers is too low and the corrosive effect of the salt bath is not present (Lampe et.al., 1993).

2.4.2 The Diffusion Zone

As a result of the diffusion of nitrogen from the surface towards the core of the steel, several reactions occur simultaneously in the diffusion zone. These include precipitation of metal nitrides, saturation of α-Fe lattices with nitrogen, residual stress generation, carbon redistribution and grain boundary phase formation.

Good hardening of the surface of alloy steels is obtained by means of a very intensive, finely dispersed precipitate of alloy nitrides. If the iron lattice contains sufficient dissolved alloy elements capable of giving rise to these nitrides, such as Al, Cr, Mo, V, etc., their precipitation is, in the main, governed by the supply of nitrogen and the nitriding temperature. In plasma nitriding, the nitrogen content of the iron lattice near the surface is very high due to the FeN condensation on the surface and the high proportion of transcrystalline nitrogen diffusion. Furthermore, this nitrogen content can be influenced by varying the composition of the treatment gas (Edenhofer, 1974b).

Most of the nitrogen atoms in the diffusion zone (nitrided case) combine with chromium in the investigated Fe-Cr-C steels to precipitate CrN, which is the main cause of the hardening effect induced by nitriding. The generation of compressive residual stresses in the nitrided case is the result of saturation of nitrogen in α-Fe and precipitation of metal nitrides, i.e. CrN. The compressive stresses and the uptake of nitrogen in the nitrided case cause carbon redistribution: the carbon atoms initially in the steel will diffuse to the stress-free regions, i.e. towards the surface and the nitriding front, leading to the decarburisation of the nitrided case, the formation of a carbon-rich zone in the nitriding front and the formation of a grain boundary phase parallel to the surface.

The hardness profile produced by nitriding reflects the quantity, size and distribution of fine scale of CrN precipitates, which are dependent upon the nitriding temperature and concentrations of chromium and carbon in the steel as well as the nitriding potential. Optimum hardness can be achieved at temperatures around 500°C. Reducing the nitriding

potential (N_2:H_2 ratio) below the threshold value leads to a significant drop in the hardening effect owing to the relatively low nitrogen uptake in the diffusion zone. Increasing carbon content of the substrate decreases the hardening effect as well. the more carbon in the steel, the more chromium is tied up in the form of carbides: thus less chromium is immediately available to form CrN during nitriding and less hardness will develop.

The development of the nitrided case is a diffusion-controlled process. The case depth exhibit a linear relation with the square root of the nitriding time. However, when the nitriding temperature is near to or higher than the tempering temperature of the steel, the relation between the case depth and square root of the nitriding time may not be linear, particularly when the nitriding time is long.

The diffusion coefficient of nitrogen is reduced as the carbon content in the substrate is increased. Increasing temperature is more effective in enhancing the diffusion of nitrogen in low carbon steels than in high carbon steels. This is because more interstitial sites are occupied by carbon in high carbon steels.

During nitriding, the nitrided case tends to expand and is restrained by the unnitrided core. As a result, a compressive residual stress develops near the surface while a tensile residual stress evolves in the core (Jones & Martin, 1977). The level of residual stresses depends not only on the plasma process condition but also on the composition of the base material. Unalloyed carbon steels show comparatively small stresses after nitriding. However, plasma nitriding of the chromium-bearing steels yielded much higher compressive residual stresses. The compressive residual stress in the nitrided case decreases with increasing carbon content in the steel, corresponding to the observed reduction of the hardening effect as the carbon content is increased. Nevertheless, no direct relationship between microhardness and residual stress level has been observed, although the origin of residual stress generation and hardness increase is similar i.e. nitrogen uptake and nitride precipitation (Sun & Bell, 1991).

Fig.2.6 shows the typical nitrogen and carbon concentration profiles of plasma-nitrided En40B steel. As a result of nitrogen uptake in the nitrided case, a decarburized zone near the surface and a carbon rich zone in the nitriding front have been developed. This

phenomenon has been observed on both conventional and gas nitrided steel and plasma nitrided steel. However, decarburization of the nitrided case is more pronounced during the plasma process than during the gaseous process owing to the cathode sputtering involved in the plasma process. As a result, the precipitation of $Fe_3(N,C)$ phase in the prior austenite grain boundaries is less pronounced in plasma nitrided steel than in gas-nitrided steel. This may account for the high ductility of the plasma-nitrided case observed by Edenhofer (1974b). With increasing nitriding temperature and time and decreasing nitriding potential the extent of decarburization increases. This explains the observed variation of the ε:γ' ratio in the compound layer with nitriding temperature, time and potential.

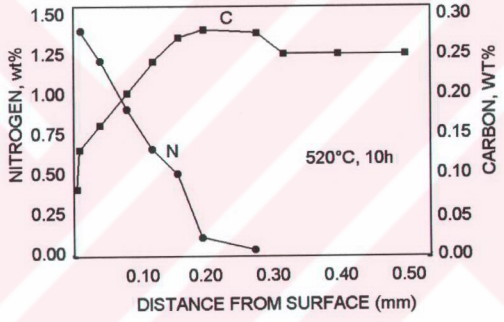

Figure 2.6 Typical nitrogen and carbon concentration profiles of a plasma nitrided steel (Sun & Bell, 1991)

2.5 THE ADVANTAGES OF PLASMA NITRIDING

The success of the plasma nitriding process led scientists in many countries to study the properties of plasma nitrided surface layers. All these studies independently agree on several major advantages of the process as compared to the conventional gas- or salt-bath nitriding techniques. The advantages most frequently mentioned can be summarized as follows:

- Completely environmentally harmless technology: Produce no toxic fumes or waste. There is no significant dirt, noise, or heat pollution

- No safety problems: There are no risks of explosion
- Reduced processing times (increased diffusion)
- Reduced energy consumption
- Reduced treatment gas consumption
- Reduced distortion
- No cleaning after the treatment.
- No grinding after the treatment
- Easy masking methods (selective treatment by using simple sheet masks)
- Treatment of the complete range of ferrous materials
- The ability to provide uniform case on complex geometry
- Superior, controllable, layer structures
- Increased service life
- The ability to impart hard wear resistance surfaces without brittleness or causing spalling or galling found with conventional nitriding
- The potential for reducing scrap through precisely repeatable cycles.

2.6 INDUSTRIAL APPLICATIONS OF PLASMA NITRIDING

In spite of excellent laboratory results, a new process will only lend itself to industrial application if its control can be supervised or automated and if the results obtained at the laboratory stage can be reproduced on industrial plant.

Various industrial plasma nitriding installations have been available since 1970`s. As well as small automatic units for plasma nitriding small parts, e.g. 6million, the balls of ball-point pens with a diameter of about 0.7 mm per day, there are a number of large installations in which components weighing several tons can be treated. There is even examples of parts to be plasma nitrided as heavy as 14 tons in the literature (Edenhofer, 1976).

Today, large-scale industrial applications of plasma nitriding are mainly found in general mechanical engineering and in the fields of engine, vehicle, gear, roller and tool production. Some examples of applications are given below :

Side and middle housings of Wankel engines are plasma nitrided in series. For the purpose of plasma nitriding, the completely finished parts, which are made of GG 25 gray cast iron, are stacked on posts. The cooling ducts are covered with sheet-metal shields, so that only the rotor contact surface will be plasma nitrided. Dimensional changes due to plasma nitriding are extremely low. The change in dimension of the above-mentioned part is less than 20μm, measured across its entire contact surface. Thus, no refinishing is required. On the understanding that the workpieces have undergone a preliminary heat treatment (stress-relieving), this high dimensional stability is due to three specific properties of the plasma nitriding process:

1. Uniform, slow heating of the workpiece in the glow discharge.
2. Uniform temperature distribution during treatment due to a constant ion-current density over the entire surface of the workpiece.
3. Slow cooling in a vacuum.

The freedom from distortion that accompanies the plasma nitriding process is one such technical factor that has influenced design engineers in the automotive sector to specify plasma nitriding as an economic and technically viable alternative to the carbonitriding of timing gears which resulted in excessive scrap levels due to quench distortion problems.

As part of this process substitution program within the automotive industry the Institut für Werkzengmaschinen der Rheinisch-Westfalishchen Technischen Hochschule, Aachen has carried out investigations on a number of plain carbon and low alloy steel gears. Standardized gears were plasma nitrided using a range of parameters and subjected to fatigue testing. Based upon the satisfactory results of these investigations, the Ford Motor Co. set up a new production line for the manufacture of timing gears used in diesel engines (Rembges, 1986; Hombeck & Bell, 1991). The production line has been designed so as to contain a completely automated plasma nitriding unit fully integrated within it. Such a system is possible because plasma nitriding is clean in environment and does not disturb the workers of the production line. This type of system can nitride up to 3500 timing gears, having a total weight of 4500 kg, in one load over a 24 h period. Up to seven different types of gears are regularly treated with varying numbers of each kind. These particular gears shown in Fig.2.7 are made from AISI 4140 steel and are plasma nitrided to produce a case

depth of 0.3 mm. Examination of the gear profile revealed a uniform monophased γ′ compound layer of typical thickness greater than 4 μm. Replacing the case hardening by plasma nitriding saves the cost for transportation, tempering and the finish machining steps which results in a cost savings of US$2 per gear.

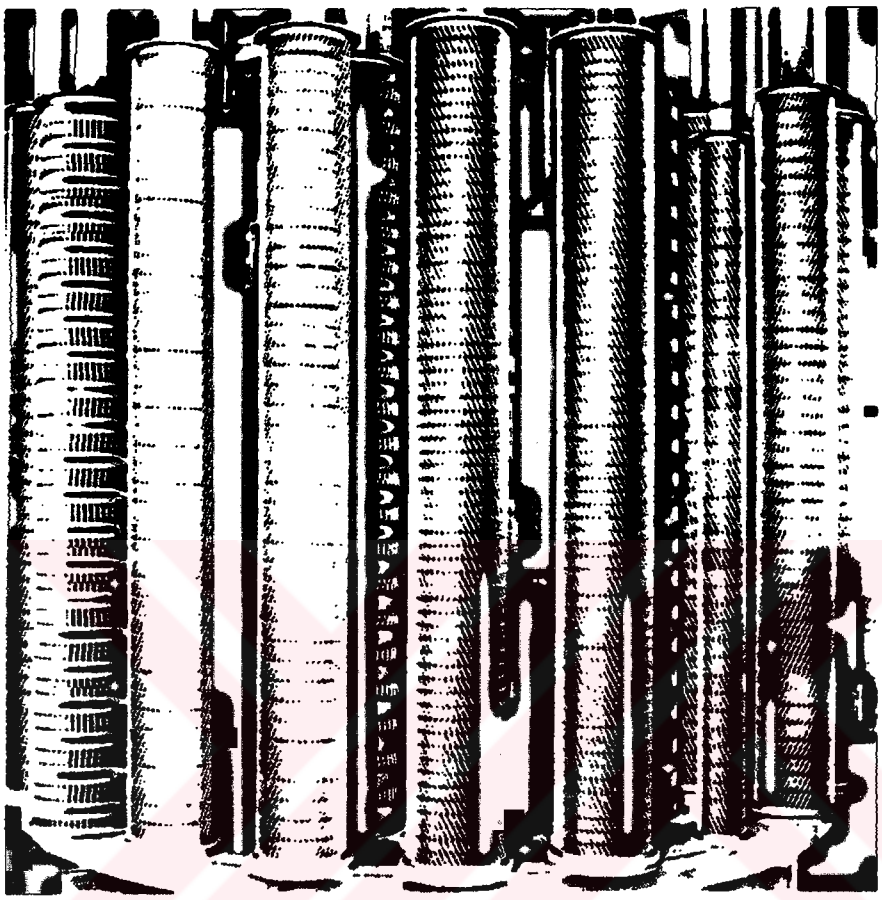

Figure 2.7 Typical load of 3500 gears made from AISI 4140 steel (Hombeck & Bell, 1991)

Further examples typical of automotive components that are being routinely treated by the plasma nitriding method are illustrated in Fig.2.8. These comprise engine valves, differential housings for four wheel drive cars, differential rods for agricultural tractors, steering ball pivots, diesel injector bodies, and other engineering components. All these components are plasma nitrided under in line production conditions or in subcontract commercial heat treatment facilities (Rembges, 1986).

Plasma nitriding technique is also utilized in tool and die making. The process is applicable with advantage to all kinds of tools, whether they are intended for hot or cold

working of metals, or for cutting, punching and chipping. The same holds true for the various tools used for the processing of plastics.

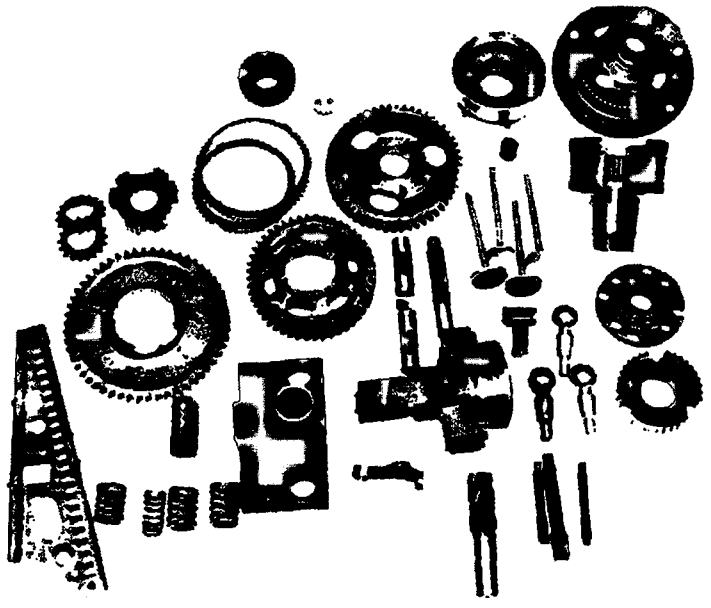

Figure 2.8 Typical automotive components that are routinely plasma nitrided

In the field of plastics processing machinery, the wear on extruding screws and cylinders has continued to increase because of the higher stresses exerted when processing thermoplastics and thermosetting plastics. Comparative measurements of the service life of gas nitrided and plasma nitrided equipment indicates that the plasma nitrided equipment lasts 5-12 times longer depending on the material. As well as small screws and cylinder, plasma nitriding furnaces have been produced capable of treating machine members up to 11m in length (Edenhofer, 1974b).

With forging dies, for example, which are usually made from hot working tool steels similar to H13, plasma nitriding treatments for 20 hours at 530°C, have been shown to give longer service lives than their 40 to 60 hour gas nitrided counterparts.

With cold working tools for rolling, bending, drawing etc. it is vital that the high core hardness of the tools developed in hardening and annealing is not reduced by the subsequent nitriding treatment. For this reason, plasma nitriding treatment, which runs at temperatures as low as 400°C, offers new possibilities for nitriding of these components.

Such cutting tools as drills, taps, millers and punches are usually manufactured from high-speed steels and hardened and annealed to about 63 to 65 HRC. A plasma nitriding treatment of 10 to 30 minutes at 500°C will usually increase the surface hardness to about dph 1200. Naturally such an extremely hard layer has low ductility. Therefore, to keep embrittlement low, it is essential that only a thin diffusion layer without any compound layer is produced. This is achieved by choosing the appropriate treatment gas with a low nitrogen concentration, by keeping temperature low (500°C) and the treatment time short (10 to 30 minutes). This kind of treatment usually improves the service life of cutting tools by a factor of 2 to 4 (Edenhofer, 1976).

2.7 ECONOMIC CONSIDERATION

The economy and productivity of the process is another important point to mention. The advanced techniques used in controlling the vacuum, the dc currents and the glow discharge account for a capital cost of the plasma nitriding plant which is higher than that of a conventional gas- or salt-bath nitriding unit. However, when all other costs, i.e. running, maintenance, labor etc., as well as the through-put of the plasma nitriding installations is taken into consideration, a cost per part is arrived at which is competitive with conventional treatments.

The running cost of plasma nitriding installations are governed by the low consumption of gas and electric energy. Because treatment takes place in a vacuum, the necessary gas flow is as low as 30 to 100 l/h (7 to 20 g/h). The vacuum also accounts for the low energy consumption as the heat loss of the charge is by radiation only. The heat is directly produced at the surface of the workpieces by means of the ion bombardment and therefore the electric energy required to heat the charge depends on the size of its surface area. To plasma-nitride, for instance, a 14 ton En1g pressure bar pin to a depth of 0.02 in required an energy input of 3000 kWh. A load of very small pieces, for example 6000 inlet valves, weighing about 1 ton in total, takes an energy of about 400 kWh to be plasma-nitrided to a depth of 0.005 in (Edenhofer, 1976).

Maintenance costs are very small as there is no wear and no nitriding of the walls of the vessel. Corrosion is no problem either, as the gases used are not corrosive. In addition there are no heating elements subject to thermal shock and no moving parts except for a standard rotary vacuum pump.

The throughput of a plasma-nitriding installation is approximately three times that of a comparable gas nitriding unit, since overall treatment times are much shorter, while the quick and easy masking methods used in plasma-nitriding treatments are other sources of appreciable cost and time savings. Additional considerable savings come after pieces leave the treatment vessel. Washing or cleaning is unnecessary.

To those cost savings, which are directly related to the working of plasma-nitriding installations, other indirect cost savings are to be added. They are produced by the longer service life, the special layer properties and the high dimensional stability. By this, machining and straightening processes are eliminated and secondary production costs as well as downtime are reduced.

All these factors add up to the positive economics of the plasma-nitriding process and have helped the fast growth of this technique within a sort time.

CHAPTER THREE
EXPERIMENTAL STUDIES

3.1 MATERIAL

Commercial AISI 5140 (DIN 41Cr4) steel was used as the test material, its chemical composition is listed in Table 3.1. As-received AISI 5140 steel rods, which had a diameter of 10 mm, was annealed at 850 °C for 1/2 h, quenched in an oil bath, heated to 580 °C for 1h and then cooled in air to room temperature.

Mechanical properties such as yield stress (σ_y), ultimate tensile strength (σ_{uts}) and elongation (ε) of quenched and tempered material were determined as 992 Mpa, 1087 Mpa, and 14% respectively.

After heat treatment, specimens for metallographic examination & microhardness testing, fatigue testing, and wear testing were machined and ground.

Table 3.1 Chemical composition of test material (AISI 5140)

Element	C	Si	Mn	S	P	Cr	Ni	Al
Amount (wt%)	0.46	0.22	0.77	0.03	0.02	1.11	0.08	0.43

3.2 PLASMA NITRIDING PROCEDURES

The plasma nitriding was carried out in a laboratory type plasma-nitriding unit (Fig.3.1) produced in Mechanical Engineering Department of Dokuz Eylül University. The unit did not allow the direct control of the current of the glow discharge. In all the treatments the

surface area of nitrided components was kept constant, so current density is proportional to current. The voltage and current density ranges were 400-600V and 2.5-4.0 mA/cm^2 depending upon the gas composition of the plasma atmosphere and required temperature. Plasma current was increased by increasing the applied voltage and increasing the N_2 concentration of the nitriding atmosphere. Upper values of applied voltage were utilized in the case of lower nitrogen concentrations and higher treatment temperatures.

a)

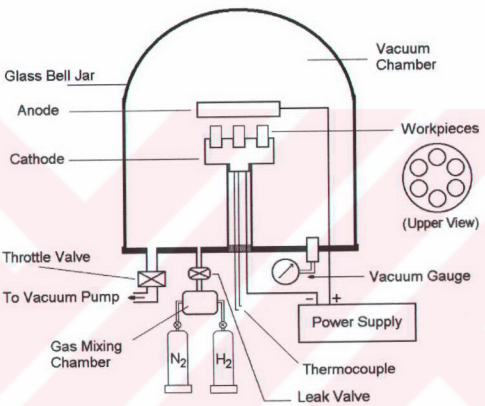

b)

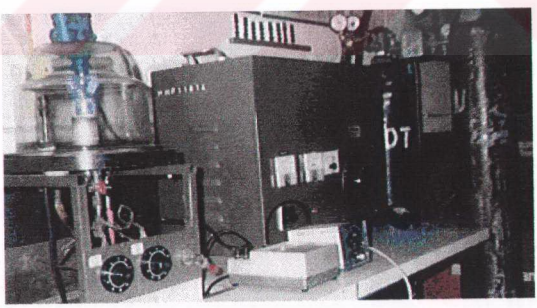

Figure 3.1 Plasma-nitriding unit used in the investigations a) Schmatic b)Photograph

The plasma nitriding process was performed as follows:

1. After cleaning in alcohol, the specimens were put into the plasma nitriding chamber and the chamber was evacuated to $2x10^{-2}$ mbar.

2. Prior to plasma nitriding, the samples were subjected to cleaning by hydrogen sputtering for 15 minutes under a voltage of 600 V and a pressure of 5 mbar to remove surface contaminants.
3. Gas mixture containing predetermined volume of Nitrogen and Hydrogen was allowed to flow into the chamber.
4. The pressure inside the chamber measured with the manometer was maintained at 10 mbar by balancing the leak rate against the vacuum pump.
5. The power supply was switched on and the voltage gradually incrased to strike a glow. Then, it was further increased to heat the specimens to the required temperature.
6. The temperature was monitored by a Ni-CrNi thermocouple inserted through the hole at the bottom of a specimen. Due to the symmetry of the specimens about the cathode axis, this temperature reading was accepted to be the temperature of all specimens being plasma nitrided together.
7. Time keeping for the process was started as soon as reaching the process temperature which took about 15 minutes after the formation of plasma.
8. All of the plasma nitriding procedures were caried out at various temperatures, times and gas compositions. Table 3.2 shows their variations relative to each other. A total gas pressure of 10 mbar was kept constant throughout the study.
9. The specimens were cooled to room temperature, before they were removed from the vacuum chamber.

Table 3.2 Plasma nitriding process conditions.

GROUP	TİME (h)	TEMPERATURE (°C)	NITROGEN (vol.%)
1.500.20	1	500	20
4.500.20	4	500	20
8.500.20	8	500	20
12.500.20	12	500	20
4.450.20	4	450	20
4.550.20	4	550	20
4.500.10	4	500	10
4.500.60	4	500	60

3.3 MICROHARDNESS TESTING AND OPTICAL MICROSCOPY

After the completion of plasma nitriding process, the microhardness specimens which had a diameter of 7mm and a length of 15mm were cut parallel to one face of the specimen surface. The cross-sections, were mounted in a cold setting resin, prepared using standard techniques and etched in 2% nital reagent. The structures were observed and photographed using an optical microscope. The thickness of compound layers were also measured during these observations.

Vickers microhardness measurements using a load of 80 gr were performed to determine case depth as well as to aid in characterizing the physical properties of the case as a function of depth from surface. Case depth at a hardness value 10% above the core hardness was taken as an accurate measure of total case depth.

Average hardness values of a minimum of three indentations at each depth were used to obtain microhardness profiles of the specimens.

Optical microscopy was also employed in fractography studies of fatigued and worn surfaces.

3.4 XRD, AND SEM STUDIES

The phases present in the surface of the nitrided layers were analysed by x-ray diffraction (XRD) using a JSDx-100 S4 X-ray diffractometer. An extra analysis of the nitride phases of a sample (12.500.20) present at a depth of 5μm from the surface was accomplished by carefully grinding the specimen surface with a 1200 grit SiC emery paper and paste. CuKα radiation was used in all XRD studies.

Scanning electron microscopy (SEM) studies were performed on selected samples to observe the microstructure of treated specimens, fractographic examination of fatigue specimens and worn surfaces of wear testing specimens.

3.5 FATIGUE TESTING

In order to investigate the fatigue behaviour of specimens, untreated and plasma nitrided using various process parameters, a number of fatigue tests were performed.

The shape and size of the fatigue testing specimen is given in Fig.3.2. In order to minimize the theoretical stress intensity factor K_t , the radius of the specimen was chosen in accordance with ASTM standards (ASTM, 1982-a).

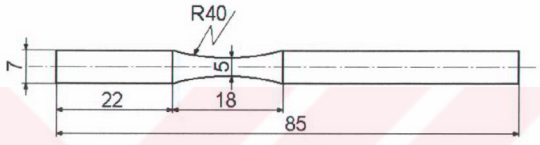

Figure 3.2 The shape and dimensions of fatigue specimens

A reversed bending fatigue machine, produced in Mechanical Engineering Department of Dokuz Eylül University, operating at 2815 rpm (about 50 Hz) was used throughout the study. A photograph of the machine is given in Fig.3.3.

The specimens were tested in a fully-reversed mode with a minimum:maximum load ratio of -1. Tests were performed at room temperature in laboratory air atmosphere. The stress was varied by changing the eccentricity of the shaft. Some specimens instrumented with strain gages were used to obtain eccentricity-maximum stress relation and calibration of the machine. This relationship was also determined by a numerical study

The specimens were tested to fracture at a given stress level. The machine stopped automatically as soon as the fracture occured. The cycles to failure was determined by an inductive counter. Endurance limits were based on runouts of $2x10^6$ cycles.

In this study a bi-linear type S-N curve was applied to the test results. This method assumes that the S-N curve consists of two linear parts, the slope part and the horizontal part. Slope part of S-N curve is the part which is determined by the data of finite fatigue life, not including the horizontal part of the S-N curve. For the slope part of S-N curves, 12 specimens were used at four different stress levels. Curve fitting method suggested by

ASTM, American Society for Testing and Materials, (ASTM,1982-b) have been utilized for the slope part of the curves. The Staircase Method (Collins, 1981) have been used for the horizontal part, the fatigue limit part of S-N curves. 9 specimens for each group were used to form the horizontal part.

The application of the bi-linear curve to the fatigue test results of a specimen group is given in Appendix as an example.

After fracture, fracture surfaces were examined by optical microscopy and scanning electron microscopy techniques. Fracture surfaces were traversed from the edge of apparent crack initiation. The mode of fracture at each point was studied, and representative photographs were taken. Special attention was paid to differentiate fracture surfaces of untreated and plasma nitrided specimens as well as crack initiation sites of specimens tested at high and low stress levels.

3.6. WEAR TESTING

Wear tests were performed on untreated and plasma nitrided specimens to determine the optimum process parameters or microstructure for maximum resistance to wear. All wear tests were caried out under dry sliding conditions at room temperature using a pin-on-ring friction and wear testing machine shown in Fig.3.4. The ring of wear couple was made of an oil quenched AISI 4140 steel having a hardness of 60±2 HRC. It had a diameter of 60mm, and a thickness of 16mm. The cylinderical surfaces of the rings were ground to a surface finish of 0.20μm (Ra).

The pins were cylinderical samples 12,7 mm long and 7 mm in diameter. After machining, flat faces of the pins were ground using 600 grit SiC emery paper.

Tests were performed with a normal load of 40 N (P_N), and a sliding speed of 0,5 $m.s^{-1}$ for a total sliding distance of 2000 m. The tests were interrupted after each 400m of sliding distance so that the wear rate of the pins could be monitored by weight loss to an accuracy of $\pm 10^{-4}$g. Pins and rings were cleaned with alcohol before the tests. The pins were also cleaned in the same way before and after each weighing.

Friction force was recorded throughout the tests, and coefficiant of friction (μ) for the mating elements was determined.

After the wear tests, wear scars were examined by optical and scanning electron microscopy (SEM) to monitor topographic features of worn areas and to investigate whether any change in wear behaviour occured as a result of plasma nitriding. Wear debris was collected and examined by optical microscopy as well.

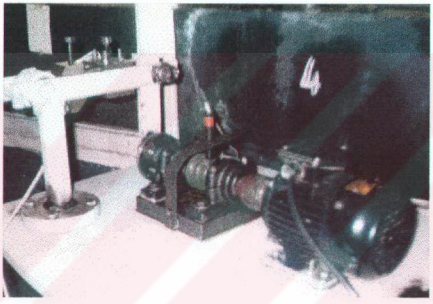

Figure 3.3 The fatigue testing machine

Figure 3.4 The wear testing machine

CHAPTER FOUR
RESULTS AND DISCUSSION

4.1 X-RAY DIFFRACTION ANALYSIS

X-ray diffraction analysis indicated that the compound layers produced by plasma nitriding mainly consisted of the γ′-Fe_4N and ε-$Fe_{2-3}N$ phases. Owing to the low chromium content (1,11 wt.%) of the material, the existence of chromium nitride is beyond the limit of detection for XRD.

Typical diffraction traces shown in Fig.4.1 illustrate the growth of the nitride phases at 500°C over different periods. A careful examination of these patterns shows that the intensity of the diffraction lines belonging to ε-nitride decreases with time, whereas that belonging to γ′-nitride increases with time.

The effect of process temperature and nitrogen concentration on the formation of surface layers can be drawn from the XRD patterns shown in Fig.4.2. By comparing the patterns belonging to specimens plasma nitrided at 450°C and 500°C (Fig.4.2a and b), it is easily seen that, the peaks of γ′ phase increases with increasing process temperature, while ε-nitride peaks decrease.

The formation of ε-nitride phase was enhanced by a high nitrogen content in the nitriding atmosphere. The XRD pattern of the specimen treated with 60vol.%N2 (Fig.4.2c) contains significantly greater amounts of ε-nitride phase compared with that treated using 20vol.%N2 (Fig.4.2b) On the other hand, γ′-nitride peaks decreases with increasing nitrogen content.

Kurny et al. (1986) observed the formation of the γ′+ ε nitrides on plasma nitrided En40B steel in a mixture of 25%N2 and 75%H2, at a temperature range of 475-550°C. In contrast, in another study (Kurny et al., 1988), he found only γ′-nitride on pure iron (Armco iron) at the same plasma nitriding conditions. The difference may be due to the carbon content of the steel. Edenhofer (1974-b) observed that the stability range of ε-nitride increases in the presence of carbon. The gradual decrease in the amount of ε-nitride in the compound layers of specimens treated for longer duration, at higher temperatures and in lower amounts of nitrogen could be attributed to the decrease in carbon content due to sputtering.

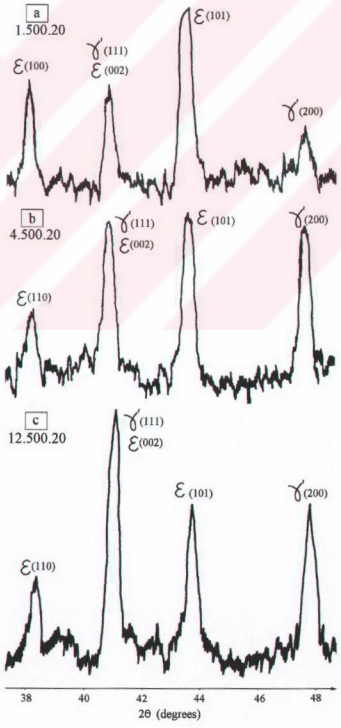

Figure 4.1 XRD patterns of specimens plasma nitrided for (a) 1h, (b) 4h and (c) 12h

Edenhofer (1974-b) has reported that during plasma nitriding, sputtering removes carbon together with other alloying elements from the workpiece. With increasing nitriding temperature and time and decreasing nitriding potential the extent of decarburisation increases (Sun & Bell, 1992). This explains the variations in the peaks of ε and γ′ nitrides in the compound layer with nitriding temperature, time and nitrogen content of the atmosphere (Fig.4.1 and 4.2).

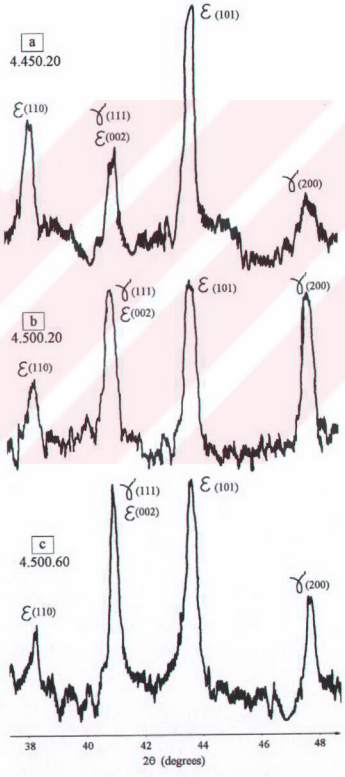

Figure 4.2 Effect of process temperature and nitrogen concentration on the XRD patterns of specimens.

Fig.4.3 shows the XRD pattern of 12.500.20 specimen before and after removal of 5μm from the surface. The spectrum for the outermost layer indicated that γ′and ε nitrides

formed on the surface (Fig.4.3a). After the removal, both γ′ and ε-nitride peaks decreased, and an α-Fe peak appeared as expected (Fig.4.3b). But, the decrease in intensities of ε peaks were more pronounced than that of γ′ peak. It can be concluded from this observation that γ′ forms at greater depths than ε-nitride, which is in agreement with an earlier finding (Chyou & Shih, 1990).

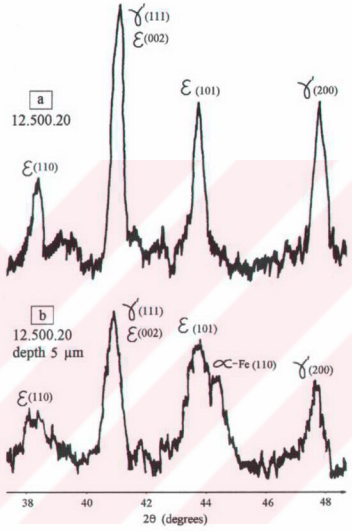

Figure 4.3 XRD pattern of the sample 12.500.20 from the surface (a), and at a depth of approx. 5μm from the surface to the core (b)

4.2 MICROSTRUCTURE AND MICROHARDNESS

Microstructural examination of plasma nitrided specimens showed formation of compound layers with different thicknesses indicating that nitriding potentials (i.e. N_2:H_2 ratio) of all groups were above the threshold value below which an iron nitride layer does not form on the surface. Effect of process temperature, duration, and nitrogen content of the plasma nitriding atmosphere on compound layer thickness can be observed on micrographs given in Fig.4.4.

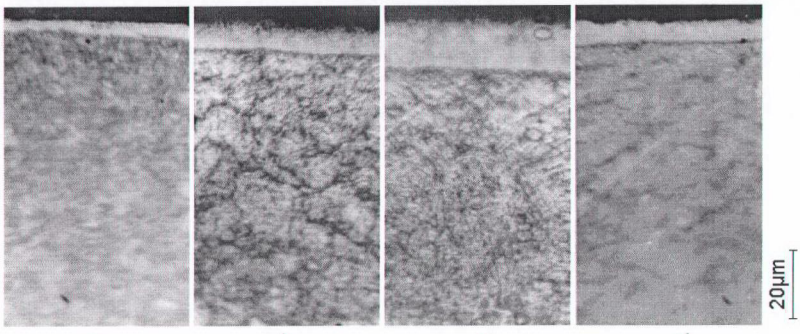

Figure 4.4 Cross-sectional optical micrographs of plasma nitrided samples a)4.500.20 b)8.500.20 c)4.550.20 d)4.500.60 (etch 2% nital)

It is clearly seen that compound layer thickness increases by increasing all these three parameters. Process temperature seems to be the most effective parameter in determining the compound layer thickness.

A SEM micrograph of the sample treated at the lowest temperature for 4h (4.450.20) is shown in Fig.4.5. The compound layer which has a thickness of approximately 2µm is clearly visible on the SEM micrograph.

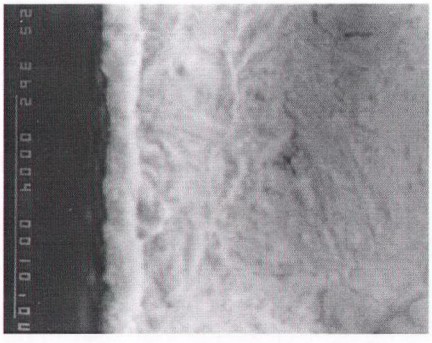

Figure 4.5 SEM micrograph of a sample treated at 450°C for 4h (4.450.20)

Average microhardness values as well as case depths and compound layer thicknesses are represented in Table 4.1 for the 8 groups of specimens considered in the study.

Table 4.1 Average values of microhardness, case depth and compound layer thickness of all specimen groups

	Specimen Groups							
Distance from surface ⇓	*1.500.20**	*4.500.20*	*8.500.20*	*12.500.20*	*4.450.20*	*4.550.20*	*4.500.10*	*4.500.60*
25	760	986	918	862	943	810	968	940
50	710	941	910	860	890	798	930	910
75	650	836	886	848	796	775	859	822
100	546	725	832	828	690	720	715	696
133	430	580	765	798	562	656	552	592
166	380	476	685	745	430	575	455	462
200	360	438	572	648	405	508	440	430
250	345	405	468	538	385	445	422	412
300		385	416	472	360	406	396	382
375							351	360
400		370	386	412	345	385	348	345
470							345	345
500		355	370	380		366		
600		345	352	368		355		
700			345	356		345		
800				345				
Case Depths (μm)	166	320	425	496	247	424	332	306
Compound Layers (μm)	2,5	5,5	6,8	7	2	11	3	7,5

(* see table 3.2 for the process conditions of the groups)

The microhardness profiles as a function of depth from the surface are shown in Fig.4.6 for all of the specimen groups

Significant surface hardening have been observed in all plasma nitrided samples. The maximum hardness levels, the shape of the hardness-depth profiles obtained in the study are similar to those obtained in plasma nitrided low alloy steels (Robino & İnal, 1983; İnal & Robino, 1982; Chyou & Shih, 1990), but different from those reported for plasma nitrided high alloy steels (Miyamura et.al., 1986; Takada et.al., 1986; Sato et.al., 1988), which show a sharp interface between the nitrided case and the core.

Effects of process parameters such as treatment temperature, duration, and nitrogen content of the atmosphere (vol.%N2) on the hardening characteristics of the specimens have been discussed below.

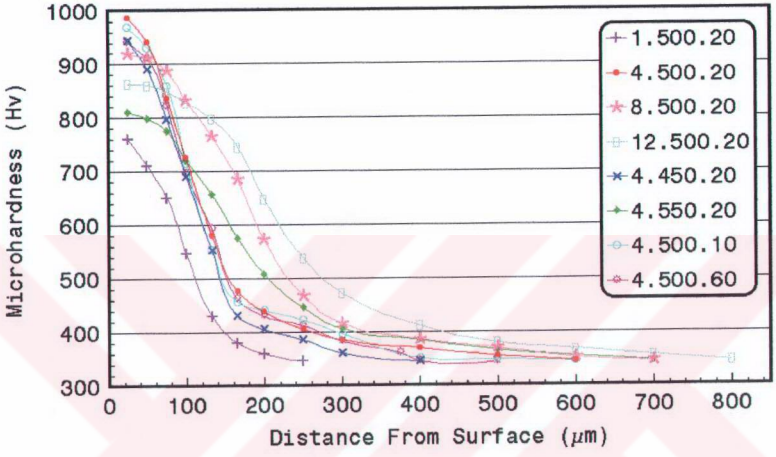

Figure 4.6 Microhardness-depth profiles of the specimens

In addition to hardness-depth curves, graphics illustrating the variations of surface hardness, case depth, and compound layer thickness versus process parameters have been presented. The surface hardness values are the ones measured at 25μm below the surfaces of cross sectional specimens, i.e. the first values the of hardness-depth curves.

Case depths have been determined from the hardness-depth values by interpolation using the definition given in Section 3.3.

The effect of treatment time on the hardness behavior of the plasma nitrided samples treated at 500°C is shown in Fig.4.7. Hardness level, case depth, and compound layer thickness are strongly affected by the process time. The maximum hardness level is observed for a treatment time of 4h and a decrease in hardness occurred for longer duration. (Fig.4.8a).

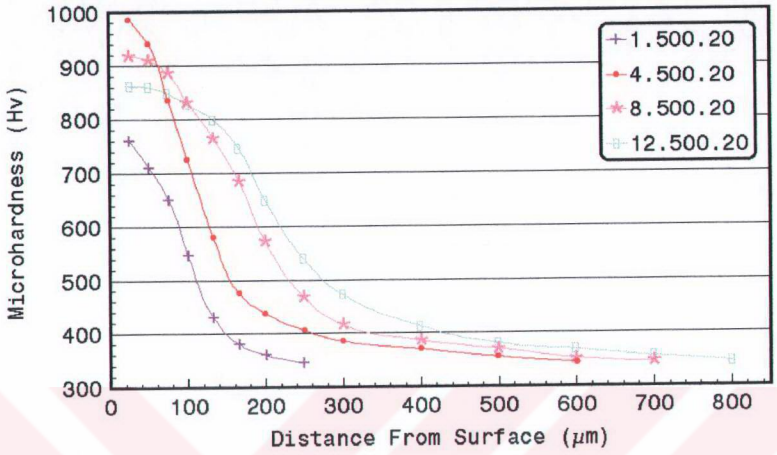

Figure 4.7 Microhardness-depth profiles of samples plasma nitrided for 1, 4, 8, and 12h

The time dependence of surface hardness is thought to be a result of precipitate size and density. For the shortest time (1h) the nitrogen uptake and precipitate density are low and therefore the amount of hardening is also low. For longer treatment times both precipitate growth and tempering of the matrix become important. As has been observed in many precipitation hardening alloys, a maximum in hardness is achieved, which corresponds to a particular aging time and temperature. This hardness is in turn related to both precipitate density and precipitate size (Robino & İnal, 1982).

Therefore, with regard to the process time, the sample plasma nitrided over a period of 4h (at 500°C) produces an optimum nitride precipitate size and density. Surface hardness of samples treated for longer duration decreased due to the coarser precipitates.

The case depth and compound layer thickness are found to be parabolic with time (Fig.4.8b). Compound layer thickness shows an increasing trend with increasing time, but it seems to reach a saturation. The saturation may be explained by surface sputtering which causes decarburisation of the surface leading to transformation of iron-nitrides from ε to γ′. This transformation has a limiting effect on compound layer thickness.

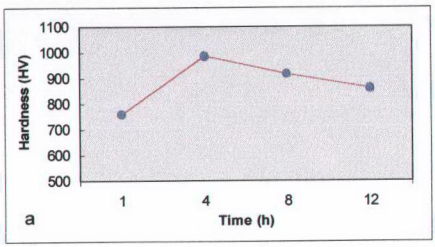

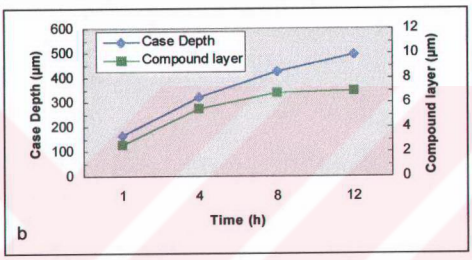

Figure 4.8 a) Surface hardness b) Case depth and compound layer thickness as a function of plasma nitriding time (1.500.20,4.500.20, 8.500.20, 12.500.20)

Typical hardness-depth profiles obtained for specimens treated in the temperature range 450-550°C are shown in Fig.4.9. For a treatment temperature of 500°C the hardness in the nitrided region is increased from the bulk value 345 to 986 HV, the maximum hardness value of all specimens. Surface hardness of the samples treated at the lowest temperature (450°C) is also quite high, but a dramatic decrease in hardness is observed on specimens treated at 550°C (Fig.4.10a).

As seen in Fig.4.10b the process temperature has a strong influence on both case depth and compound layer thickness. Both case depth and compound layer thickness increased greatly with increasing treatment temperature for the fixed treatment time of 4h due to an increased rate of nitrogen diffusion. The maximum compound layer thickness of all the samples investigated was measured on the sample treated at 550°C.

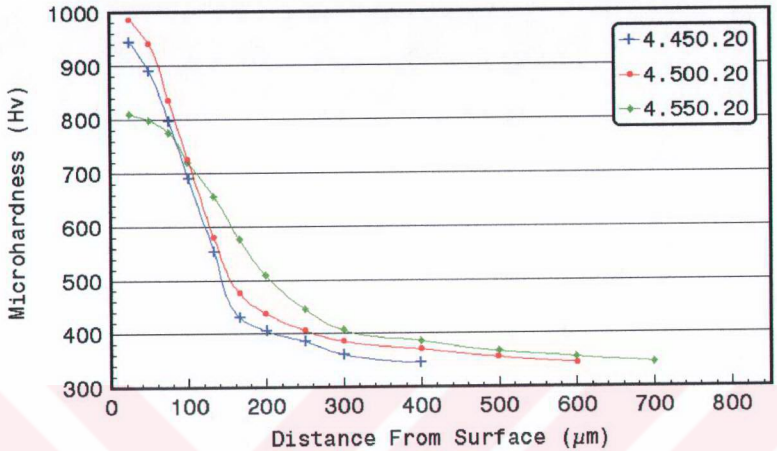

Figure 4.9 Microhardness-depth profiles of samples plasma nitrided at 450, 500 and 550 °C

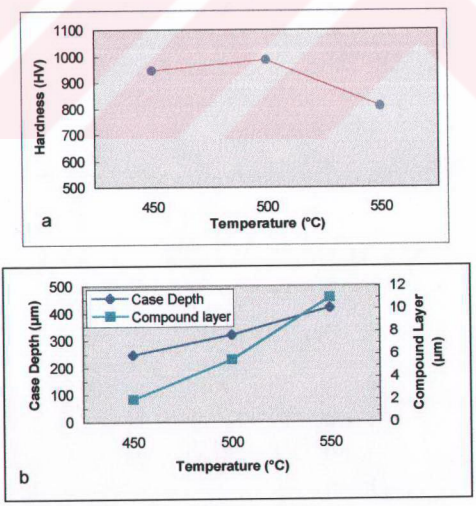

Figure 4.10 a) Surface hardness b) Case depth and compound layer thickness as a function of plasma nitriding temperature (4.450.20, 4.500.20, 4.550.20)

Differences in the hardness of the layers are generally correlated to the size, shape and distribution of the nitride precipitates in the layer. At low temperatures, since the mobility of substitutional solutes is low, a growth limited situation prevails and leads to a low precipitate density and a consequent lower hardness of the layer.

Higher nitriding temperatures correspond to higher mobility of the substitutional solutes, but here a nucleation limited situation prevails. Therefore the precipitates are larger, again resulting in lower hardness. In addition, there is a tendency for the solubility of nitrides in the matrix to increase at higher temperatures. Thus in a qualitative way it is possible to consider the magnitude of hardness in the nitrided layer to be a function of temperature. With regard to the nitriding of AISI 5140 steel over a 4h period, a temperature of 500°C produces an optimum nitride precipitate size and density. Also, at higher temperatures the tempering effect may reduce the hardness of both the case and the core.

The effect of nitriding temperature on the hardness profiles, case depths, and compound layer thickness gives an indication of the kinetics of the reaction in the nitrided layer. As the plasma nitriding parameters such as pressure and gas composition are constant for the samples in question, temperature of the specimens were adjusted by adjusting the applied voltage.

Upon increasing the applied voltage, the amount of ionized gases and the kinetic energies of the ions increases. As a result, an increase in the current and in the temperature of the samples are observed as well.

By increasing the temperature, the rate of formation of FeN complexes and their redeposition on the surface is increased, leading to growth of the compound layer. Increasing process temperature increases the thickness of the diffusion layer (case depth) by increasing the rate of nitrogen diffusion through the layer.

An increase in the applied voltage has also the effect of increasing the amount of sputtering that a sample surface undergoes during the process. As a result of increasing the voltage, i.e. process temperature, the amount of sputter cleaning taking place on the surface, which removes impurities such as oxide, increases. The enhanced removal of

contaminants from the surface could increase its reactivity with nitrogen, thus allowing more nitrogen to react and producing thicker layers.

Nitrogen content of the plasma nitriding atmosphere seems to have no significant influence on hardness-depth profiles of the samples (Fig.4.11). There does not seem to be any obvious correlation between N_2 content of the gas mixture and surface hardness levels (Fig.4.12a). The case depths were similar for all the ratios of N_2 to H_2, but seems to slightly decrease as the amount of N_2 increases. On the other hand, compound layer thickness showed a significant increase with increasing N_2 content (Fig.4.12b).

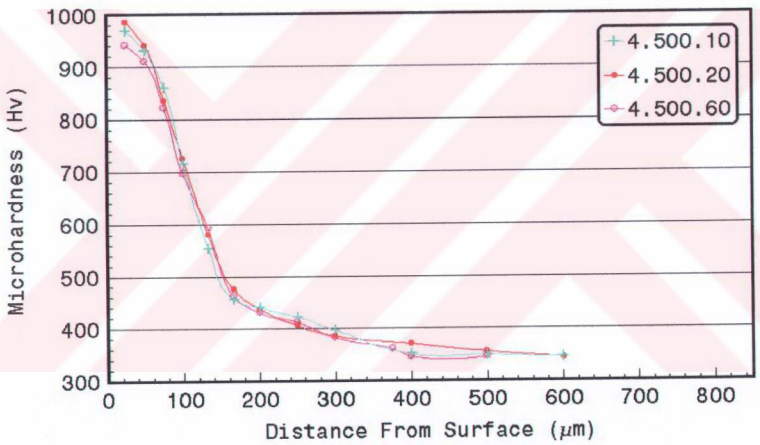

Figure 4.11 Microhardness-depth profiles of samples plasma nitrided in atmospheres containing 10, 20, and 60 vol.% N_2 at 500°C for 4h

The increase in the compound layer thickness due to the increase of N_2 concentration in the nitriding atmosphere appears to be an effect of voltage. The voltage required to keep the workpieces at the process temperature of 500°C were decreased with increasing N_2 concentration, which decreased the sputtering effect of the ions hitting the workpiece surface. As a result of this, compound layer thickness increased with increasing N_2 concentration. On the other hand, higher sputtering effect prevents compound layer from growing on the samples treated in lower N_2 concentrations.

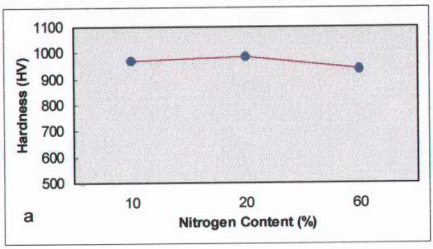

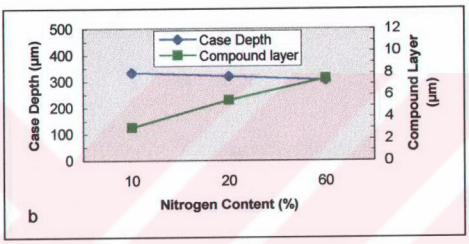

Figure 4.12 a) Surface hardness b) Case depth and compound layer thickness as a function of N_2 content in plasma nitriding atmosphere (4.500.10, 4.500.20, 4.500.60)

The slight decrease in case depth with increasing N_2 concentration can also be explained as an influence of the applied voltage. Decreasing nitrogen activity in the plasma due to the lower applied voltage may lead to decreasing case depths.

4.3 FATIGUE TESTS

4.3.1 S-N Curves

Fatigue test data of untreated and plasma nitrided specimen groups are presented in Tables 4.2-4.10. Each group has 21 fatigue data; 12 for the slope part and 9 for the horizontal part of the bi-linear type S-N curve used in this study. The application of the bi-

linear curve fitting to the fatigue test results of 4.500.20 specimens is given in Appendix as an example.

The stress-life data points and bi-linear curve fittings are plotted on S-LogN diagrams given in Fig.s 4.13-4.21 for each groups. Results of the curve fitting study containing LogN=A+B.S relations (for the slope parts) and estimates of endurance limits (S_e) are also included in these figures. As can be seen in the figures the curves fit fairly well to the data. It is also seen that the scatter increases with decreasing stress level.

S-N curves of all the groups are given in Fig.4.22. It is clearly seen that significant improvements in the fatigue strength of AISI 5140 steel may be obtained by the plasma nitriding process in comparison with untreated specimens.

For a comparative study, the S-N curves are classified according to process time, temperature, and gas composition and given in Fig.s 4.23, 4.24, and 4.25 respectively. The curve representing the untreated (quenched and tempered) specimens is also plotted for comparison.

It is clearly seen that, fatigue strength of the steel increases with increasing process time, i.e. increasing case depth (Fig.4.23). A very significant increase in fatigue strength was observed even after a treatment time of 1 hour. Improvements of 13% and 38% in fatigue limit were achieved for nitriding times 1h and 12h which correspond to case depths of 0.166 and 0.496 mm respectively (see Table 4.1). It is also seen that the knee points move forward, and slopes slightly decreases for the increasing times.

As demonstrated in Fig.4.25 all the specimens exhibited a similar fatigue behavior irrespective of the nitrogen content of plasma atmosphere. Slightly lower fatigue strength of 4.500.60 specimens may be related to their slightly lower surface hardness in comparison with 4.500.10 and 4.500.20 samples (see Fig.4.11). Unlike nitrogen content, process temperature has an important role in determining the fatigue strength of the specimens (Fig.4.24). The increase in fatigue strength with increasing temperature is obviously due to the increasing case depth.

Table 4.2 Fatigue test data of untreated specimens

Specimen Number	S, Stress (Mpa)	N, Life (Cycles)
unt-1	640	52400
unt-2	640	55600
unt-3	610	63700
unt-4	610	69400
unt-5	610	81600
unt-6	580	82300
unt-7	580	93400
unt-8	580	112500
unt-9	550	125800
unt-10	550	109300
unt-11	550	133700
unt-12	550	185300
unt-13	470	628700
unt-14	454	$> 2x10^6$
unt-15	470	$> 2x10^6$
unt-16	486	$> 2x10^6$
unt-17	502	226400
unt-18	486	489200
unt-19	470	$> 2x10^6$
unt-20	486	195300
unt-21	470	841600

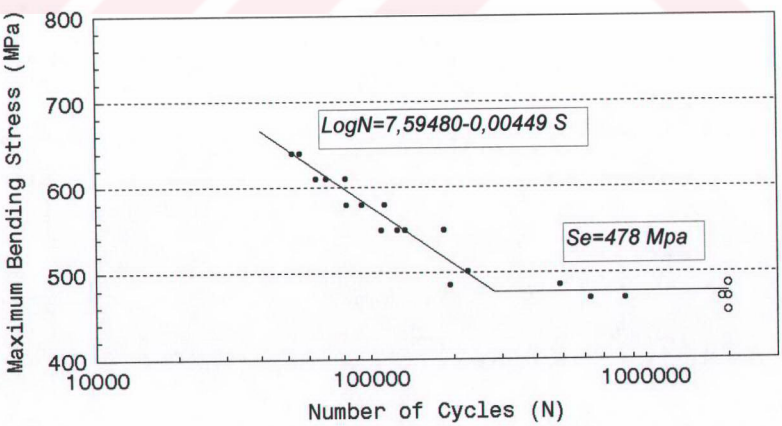

Figure 4.13 S-N curve for untreated specimens

Table 4.3 Fatigue test data of specimens plasma nitrided for 1 hour (1.500.20)

Specimen Number	S, Stress (Mpa)	N, Life (Cycles)
1.500.20-1	650	56900
1.500.20-2	650	62100
1.500.20-3	625	73400
1.500.20-4	625	76500
1.500.20-5	625	91200
1.500.20-6	600	126500
1.500.20-7	600	108500
1.500.20-8	600	90700
1.500.20-9	575	244300
1.500.20-10	575	212600
1.500.20-11	575	180700
1.500.20-12	575	122200
1.500.20-13	530	284900
1.500.20-14	514	$> 2x10^6$
1.500.20-15	530	1228500
1.500.20-16	514	$> 2x10^6$
1.500.20-17	530	$> 2x10^6$
1.500.20-18	546	187000
1.500.20-19	530	643200
1.500.20-20	514	$> 2x10^6$
1.500.20-21	530	$> 2x10^6$

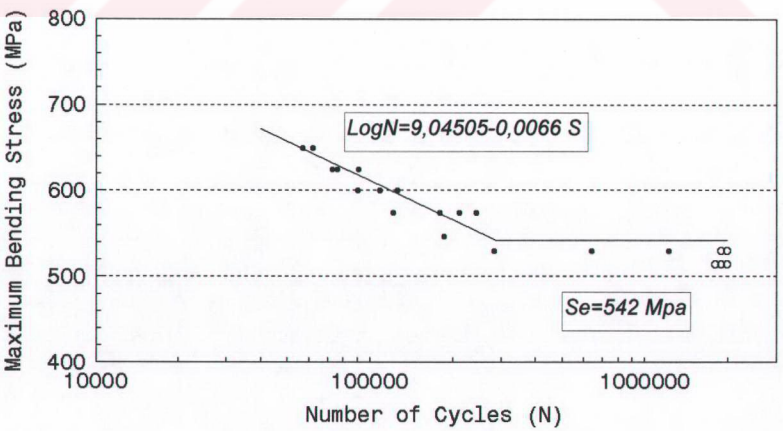

Figure 4.14 S-N curve for specimen group 1.500.20

Table 4.4 Fatigue test data of specimens plasma nitrided for 4 hours (4.500.20)

Specimen Number	S, Stress (Mpa)	N, Life (Cycles)
4.500.20-1	700	48600
4.500.20-2	700	52400
4.500.20-3	675	65700
4.500.20-4	675	79800
4.500.20-5	675	91400
4.500.20-6	650	86500
4.500.20-7	650	98600
4.500.20-8	650	133400
4.500.20-9	625	142300
4.500.20-10	625	171800
4.500.20-11	625	235700
4.500.20-12	625	343500
4.500.20-13	590	$> 2x10^6$
4.500.20-14	606	328700
4.500.20-15	590	$> 2x10^6$
4.500.20-16	606	472300
4.500.20-17	590	1050600
4.500.20-18	572	$> 2x10^6$
4.500.20-19	590	$> 2x10^6$
4.500.20-20	606	721400
4.500.20-21	590	691300

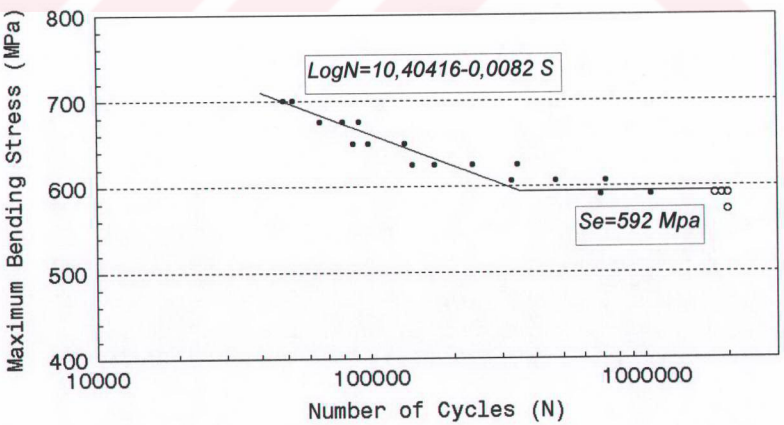

Figure 4.15 S-N curve for specimen group 4.500.20

Table 4.5 Fatigue test data of specimens plasma nitrided for 8 hours (8.500.20)

Specimen Number	S, Stress (Mpa)	N, Life (Cycles)
8.500.20-1	725	66400
8.500.20-2	725	56400
8.500.20-3	700	111400
8.500.20-4	700	87600
8.500.20-5	700	76300
8.500.20-6	675	128200
8.500.20-7	675	101600
8.500.20-8	675	173400
8.500.20-9	650	166500
8.500.20-10	650	380400
8.500.20-11	650	284500
8.500.20-12	650	263300
8.500.20-13	590	$> 2x10^6$
8.500.20-14	606	$> 2x10^6$
8.500.20-15	622	475800
8.500.20-16	606	$> 2x10^6$
8.500.20-17	622	817400
8.500.20-18	606	1427500
8.500.20-19	590	$> 2x10^6$
8.500.20-20	606	$> 2x10^6$
8.500.20-21	622	648700

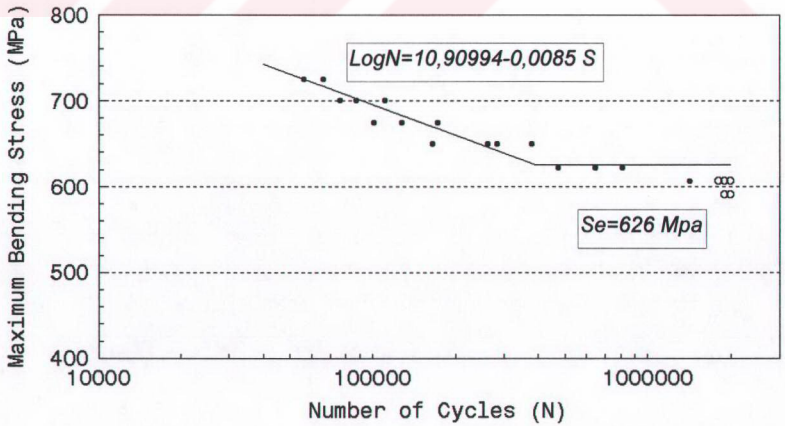

Figure 4.16 S-N curve for specimen group 8.500.20

Table 4.6 Fatigue test data of specimens plasma nitrided for 12 hours(12.500.20)

Specimen Number	S, Stress (Mpa)	N, Life (Cycles)
12.500.20-1	765	49700
12.500.20-2	765	54200
12.500.20-3	740	94300
12.500.20-4	740	61900
12.500.10-5	740	68300
12.500.20-6	715	208700
12.500.20-7	715	129200
12.500.20-8	715	8900
12.500.20-9	690	445900
12.500.20-10	690	228600
12.500.20-11	690	287900
12.500.20-12	690	187400
12.500.20-13	670	$> 2x10^6$
12.500.20-14	686	341000
12.500.20-15	670	755200
12.500.20-16	654	882600
12.500.20-17	638	$> 2x10^6$
12.500.20-18	654	1370100
12.500.20-19	638	$> 2x10^6$
12.500.20-20	654	$> 2x10^6$
12.500.20-21	670	395400

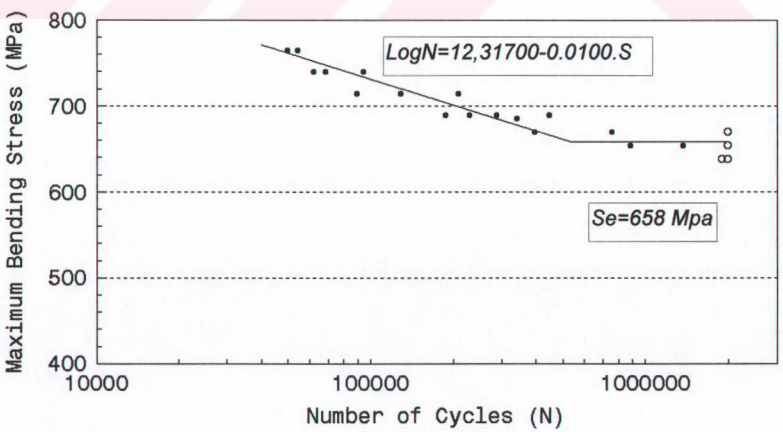

Figure 4.17 S-N curve for specimen group 12.500.20

Table 4.7 Fatigue test data of specimens plasma nitrided at 450°C (4.450.20)

Specimen Number	S, Stress (Mpa)	N, Life (Cycles)
4.450.20-1	680	44200
4.450.20-2	680	57800
4.450.20-3	655	61700
4.450.20-4	655	84700
4.450.20-5	655	77400
4.450.20-6	630	81400
4.450.20-7	630	85900
4.450.20-8	630	121600
4.450.20-9	605	114300
4.450.20-10	605	149800
4.450.20-11	605	250200
4.450.20-12	605	307600
4.450.20-13	550	$> 2x10^6$
4.450.20-14	566	773400
4.450.20-15	550	497500
4.450.20-16	534	1417900
4.450.20-17	518	$> 2x10^6$
4.450.20-18	534	$> 2x10^6$
4.450.20-19	550	954100
4.450.20-20	534	$> 2x10^6$
4.450.20-21	550	$> 2x10^6$

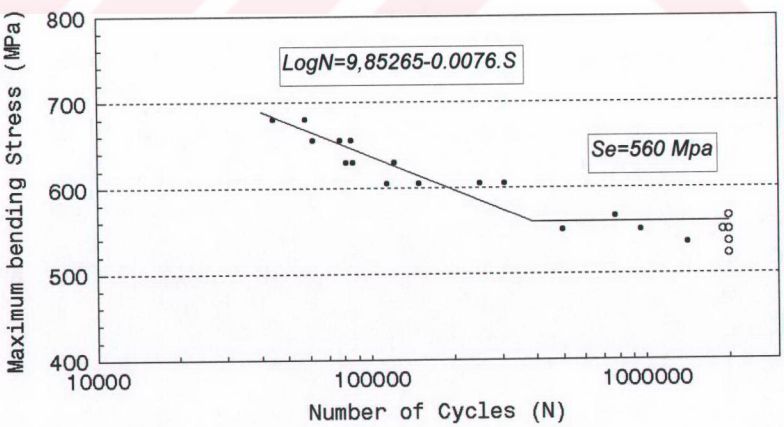

Figure 4.18 S-N curve for specimen group 4.450.20

Table 4.8 Fatigue test data of specimens plasma nitrided at 550°C (4.550.20)

Specimen Number	S, Stress (Mpa)	N, Life (Cycles)
4.550.20-1	725	47500
4.550.20-2	725	53700
4.550.20-3	700	75400
4.550.20-4	700	98700
4.550.20-5	700	118600
4.550.20-6	675	93800
4.550.20-7	675	121700
4.550.20-8	675	191000
4.550.20-9	650	143500
4.550.20-10	650	214300
4.550.20-11	650	246400
4.550.20-12	650	323700
4.550.20-13	600	$> 2x10^6$
4.550.20-14	616	655800
4.550.20-15	600	$> 2x10^6$
4.550.20-16	616	477300
4.550.20-17	600	896000
4.550.20-18	584	1236500
4.550.20-19	568	$> 2x10^6$
4.550.20-20	584	$> 2x10^6$
4.550.20-21	600	$> 2x10^6$

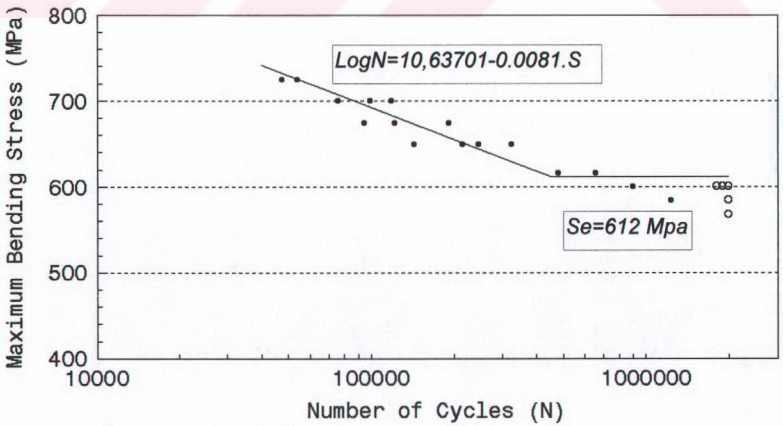

Figure 4.19 S-N curve for specimen group 4.550.20

Table 4.9 Fatigue test data of specimens plasma nitrided in atmospheres containing 10vol.%N_2 (4.500.10)

Specimen Number	S, Stress (Mpa)	N, Life (Cycles)
4.500.10-1	700	52600
4.500.10-2	700	57100
4.500.10-3	675	74700
4.500.10-4	675	66500
4.500.10-5	675	92300
4.500.10-6	650	89800
4.500.10-7	650	114200
4.500.10-8	650	152900
4.500.10-9	625	137400
4.500.10-10	625	226400
4.500.10-11	625	164100
4.500.10-12	625	321000
4.500.10-13	590	$> 2x10^6$
4.500.10-14	606	416800
4.500.10-15	590	$> 2x10^6$
4.500.10-16	606	879600
4.500.10-17	590	742300
4.500.10-18	574	874900
4.500.10-19	558	$> 2x10^6$
4.500.10-20	574	$> 2x10^6$
4.500.10-21	590	1128500

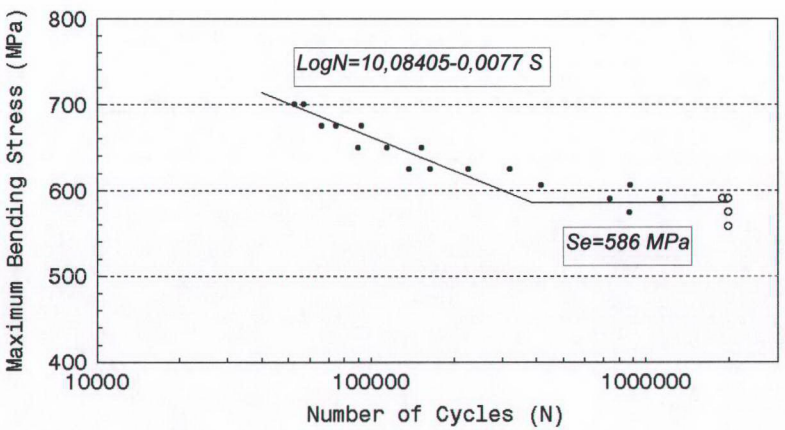

Figure 4.20 S-N curve for specimen group 4.500.10

Table 4.10 Fatigue test data of specimens plasma nitrided in atmospheres containing 60vol.%N_2 (4.500.60)

Specimen Number	S, Stress (Mpa)	N, Life (Cycles)
4.500.60-1	700	47300
4.500.60-2	700	42500
4.500.60-3	675	63600
4.500.60-4	675	70800
4.500.60-5	675	82500
4.500.60-6	650	79800
4.500.60-7	650	94600
4.500.60-8	650	125500
4.500.60-9	625	123800
4.500.60-10	625	287900
4.500.60-11	625	182100
4.500.60-12	625	115400
4.500.60-13	590	376200
4.500.60-14	574	$> 2.10^6$
4.500.60-15	590	671900
4.500.60-16	574	549100
4.500.60-17	558	$> 2.10^6$
4.500.60-18	574	1050600
4.500.60-19	558	$> 2.10^6$
4.500.60-20	574	$> 2.10^6$
4.500.60-21	590	431700

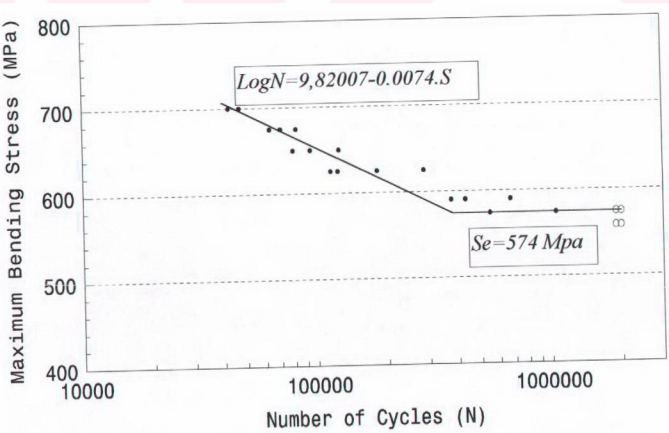

Figure 4.21 S-N curve for specimen group 4.500.60

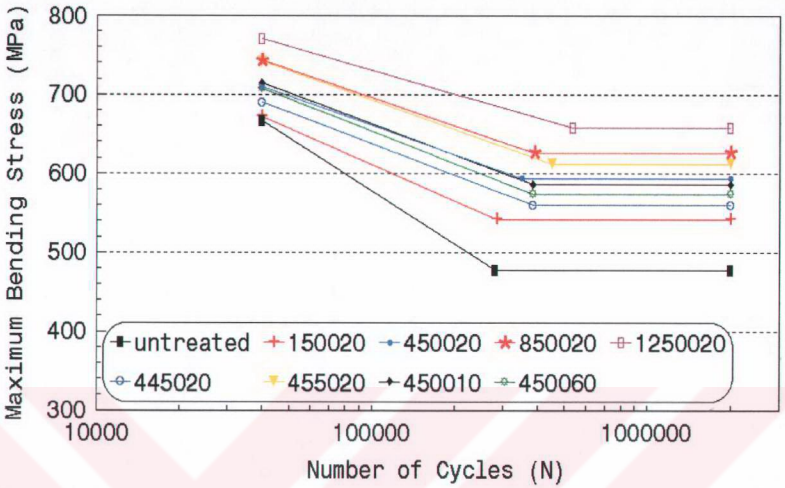

Figure 4.22 S-N Curves of all the specimen groups

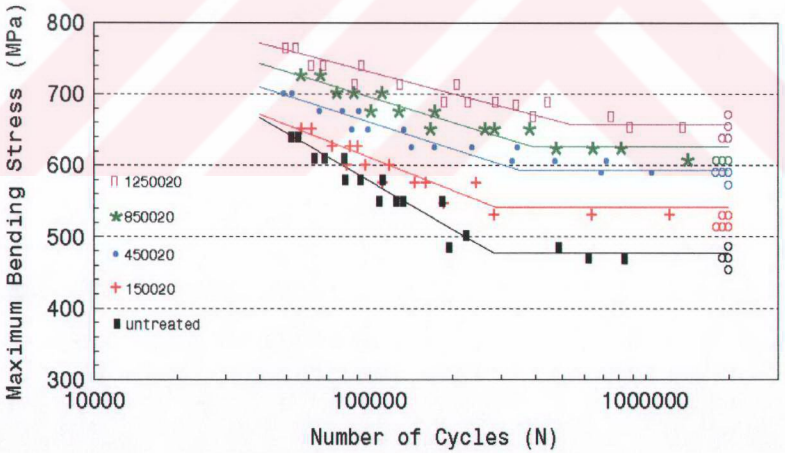

Figure 4.23 S-N curves of specimens plasma nitrided for 1, 4, 8, and 12h

The compressive residual stresses in the nitrided case, which form as a result of the saturation of nitrogen in α-Fe and precipitation of metal nitrides, increases with increasing process temperature and /or time. The residual stress pattern consists of compression at the

surface and tension at the interior (Fig.4.26). The maximum externally applied tensile stress at the surface is reduced by an amount equal to the surface compressive residual stress. The peak tensile stress is displaced to the case-core transition zone, which becomes the preferential site for crack initiation especially at low stress levels.

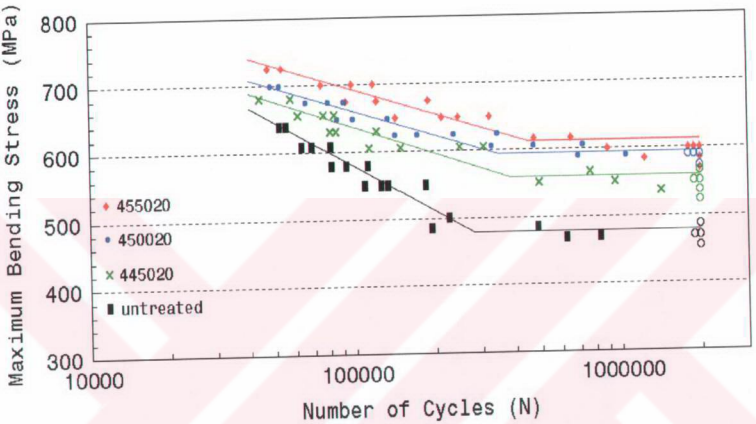

Figure 4.24 S-N curves of specimens plasma nitrided at 450, 500, and 550°C

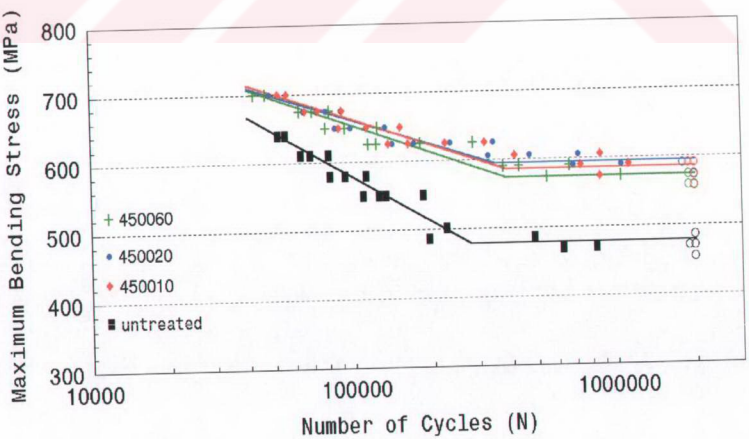

Figure 4.25 S-N curves of specimens plasma nitrided in various N_2 concentrations

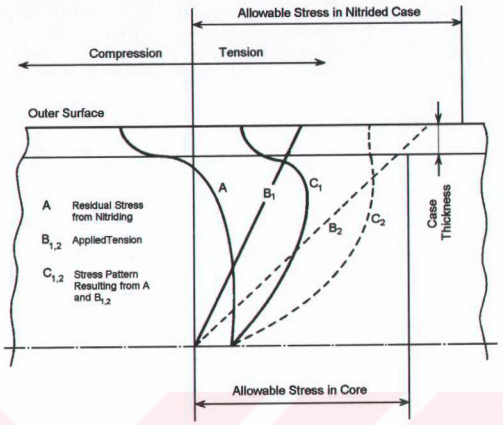

Figure 4.26 Stress pattern in the tension side of a surface-hardened bar in bending (schematic)

The effect of increasing case depth can be viewed as effectively moving the fatigue crack initiation site further into the core, indicating that a greater applied bending stress will be required at the surface to create a sufficiently high level of stress at the case-core interface to initiate failure (Sun&Bell,1991).

Since the nitrided case, a higher strength material, is produced on the surface by plasma nitriding, it can not be considered that the higher fatigue properties are due exclusively to the formation of favorable compressive residual stresses produced in the surface.

The case prevents the movement of slip bands, the intrusions and extrusions of which are the initiation sites for cracks according to a well-accepted theory of fatigue. Therefore, the slip bands can only be activated by very high stresses in the case.

Formation of the harder and stronger surface, the case, on the material supplies limiting conditions for the initiation and propagation of a crack. Thus, subsurface initiation of failure is possible under these conditions. The suppression of the slip band formation at the surface delays or decelerates the crack initiation and propagation, i.e. improves the fatigue strength of the material.

4.3.2 Fractography

Crack initiation sites has been observed as the main difference between fatigue fracture surfaces of untreated and plasma nitrided specimens

For many common loading situations including the loading conditions used here, the maximum stress within a component occurs at its surface.

Investigation of the fracture surfaces of untreated specimens revealed that, all of the cracks leading to fatigue failure originated at surface, as expected.

Fig.4.27 shows crack initiation, propagation, and final fracture regions of an untreated specimen which failed at 841600 cycles (sample Unt-17). Some imperfections acting as stress concentrators seem to initiate the fatigue crack at the surface (Fig.4.27a).

In the stage of crack propagation, a mostly transgranular cracking was the main fracture mode with typical fatigue striations (Fig.4.27b). The fracture surface here is similar to overload failure except it contains many areas which exhibit distinct fatigue striations

The fracture mode observed in the final fracture regions of untreated specimens was ductile with microvoids and dimples of non -uniform size (Fig.4.27c).

Fatigue fractography investigation of plasma nitrided specimens revealed subsurface crack initiation especially at stresses corresponding to long lives. This effect has been reported in push-pull fatigue of nitrided specimens by Jones and Martin (1978), in rotating-bending fatigue of nitrided specimens by Çelik and Karadeniz (1995) and Sun and Bell (1991).

The reason for the nucleation of the cracks below the surface is obviously the strengthening of the surface material and generation of the compressive residual stresses on the surface.

a)

b)

c)

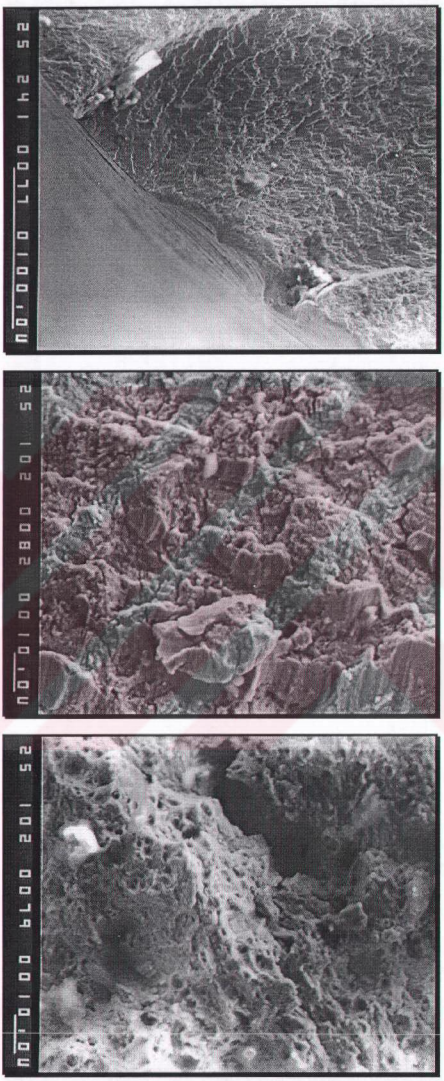

Figure 4.27 SEM fractographs of an untreated specimen with a life of 841600 cycles (Sample unt-17) a) Fatigue crack initiation area, b) well away the point of crack initiation (crack propagation area), c) final fracture region

Some micrographs of subsurface crack initiation areas in plasma nitrided specimens are shown in Fig.4.28.

The crack initiation site in Fig.4.28f (Sample 4.550.20-3) and its mating part are shown enlarged in Fig.4.29. The particle-matrix decohesion and localized deformation, which seem to be the cause of crack initiation, are evident. The particle which was fractured and had a diameter of approximately 12 μm is probably a non-metallic inclusion. Inclusions introduce localized strain concentrations because of the mismatch of mechanical, physical and chemical properties with the surrounding material (Miller, 1993).

Initially the crack growth is in along just one crystallographic plane of each grain, probably a slip plane. When the crack reaches a certain length, the direction of crack growth slightly changes, the crystallographic mode ends and striation fracture begins.

Initial crack surface through the hardened case is entirely transgranular. The appearance of fracture surface, although still transgranular, becomes coarser through the core (see Fig.4.28).

The fracture surface shown in Fig.4.30 exhibit transgranular fracture, with classic fatigue striations as is often observed in crack propagation areas of materials. Striations were more visible in the core region than in the hardened case due to the higher ductility of the core.

The final fracture surface does not show any evidence of fatigue crack growth on a microscopic level. As shown in Fig.4.31, this region is similar to the area of an overload failure, which shows the typical ductile overload fracture surface with void growth and coalescence and is free of any evidence of fatigue striations.

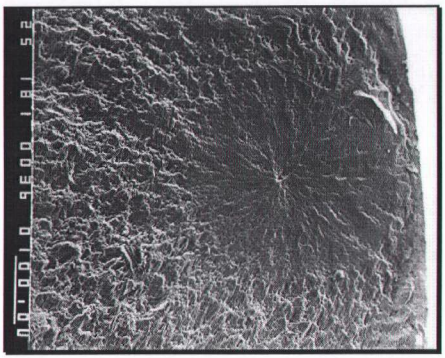

a) Sample 1.500.20-11 (N=180700 cycles)

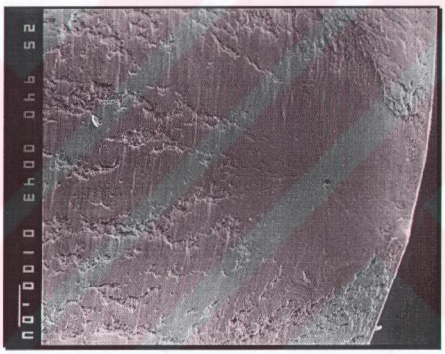

b) Sample 1.500.20-19 (N=643200 cycles)

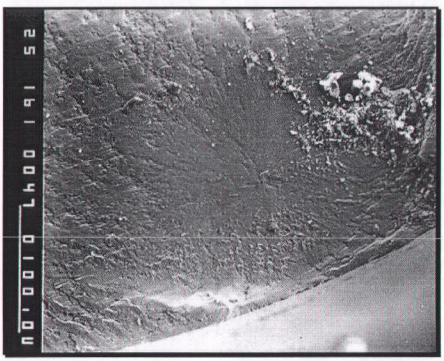

c) Sample 4.450.20-15 (N=497500 cycles)

Figure 4.28 .....continued

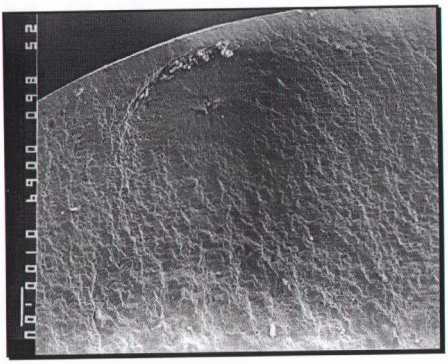

d) Sample 4.550.20-3 (N=75400 cycles)

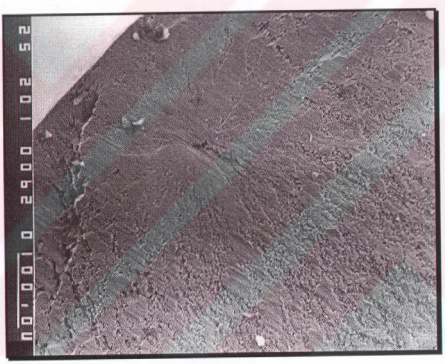

e) Sample 4.550.20-12 (N=323700)

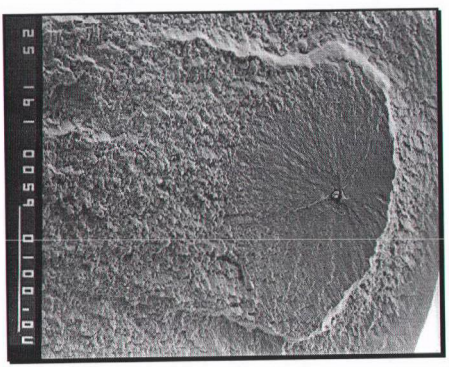

f) Sample 8.500.20-6 (N=128200)

Figure 4.28 SEM micrographs of some subsurface crack initiation areas

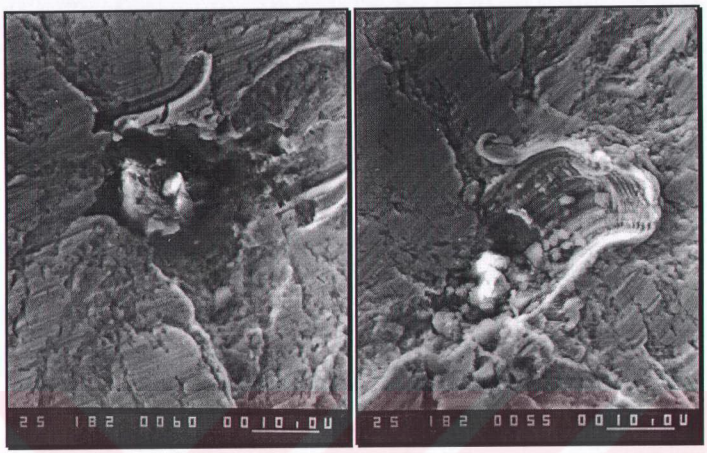

Figure 4.29 Fracture origin of Sample 8.500.20-6 and its mating part showing particle-matrix decohesion and deformation at a subsurface non-metallic inclusion

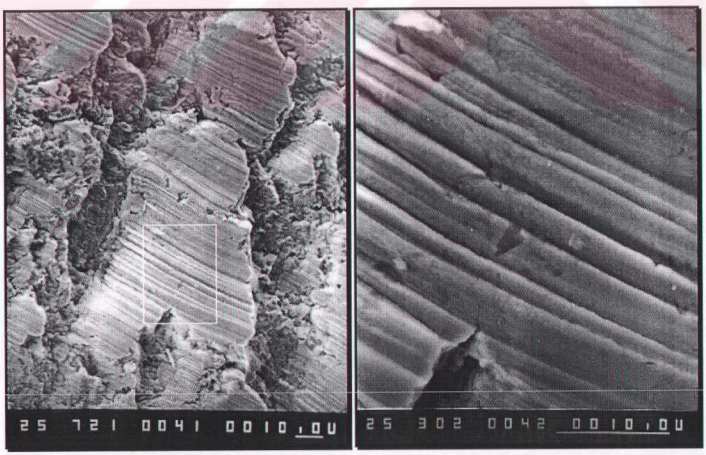

Figure 4.30 SEM fractography showing typical fatigue striations at about 2,2 mm from the crack initiation area (Sample 1.500.20-19)

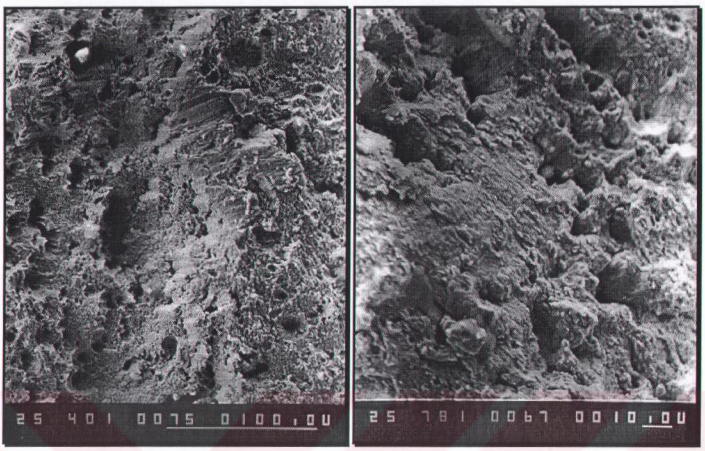

Figure 4.31 SEM fractographs of the typical fracture surface throughout the final fracture region showing dimple craters and inclusions

4.4 WEAR TESTS

Pin-on-ring wear data of untreated and plasma nitrided specimens, tested under a load of 40N for a total sliding distance of 2000m, are summarized in Table 4.11. Plasma nitriding reduced the wear rate of the material. The maximum improvement was achieved for the specimens plasma nitrided at 500°C for 4 hours (4.500.20).

The changes in weight loss for the pins as a function of the sliding distance are shown in Fig.4.32. The beneficial effect of treatment under the loading conditions employed in the present work is illustrated in this graph. It is evident that plasma nitriding substantially improves the wear performance of the steel and the degree of improvement depends on the plasma nitriding process conditions.

The coefficient of friction μ was measured continuously during the wear tests. The charts of μ vs. sliding distance showed that average coefficient of friction values of plasma nitrided samples were slightly greater than those of the untreated samples. Therefore the

improvements in the wear resistance can be related to mechanical properties rather than sliding properties of plasma nitrided samples.

Table 4.11 Average weight loss values of wear specimens

Sliding Distance(m)	untreated	1.500.20	4.500.20	12.500.20	4.450.20	4.550.20	4.500.60
400	8,85	3,66	2,36	2,47	3,12	5,23	2,55
800	14,76	5,78	3,27	4,83	4,35	6,57	4,03
1200	20,43	9,34	4,12	6,33	5,56	8,45	4,88
1600	25,18	13,36	5,22	7,49	7,1	10,2	5,87
2000	29,19	17,13	6,37	8,02	8,43	12,1	7,42

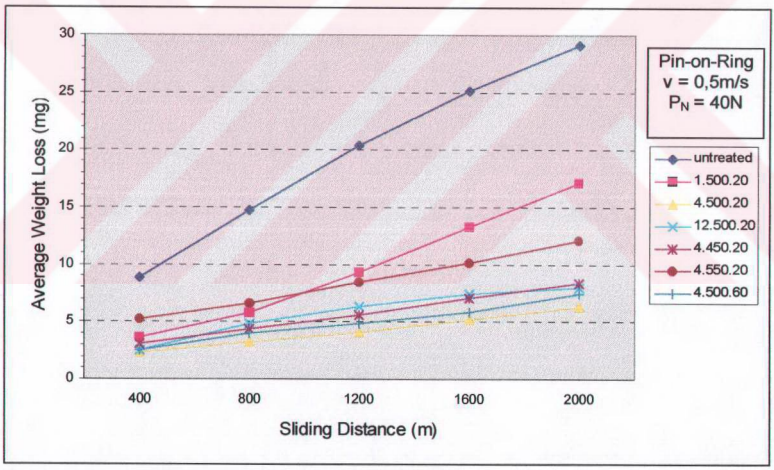

Figure 4.32 Wear curves for untreated and plasma nitrided specimens

Among the treated groups, it can be seen that initial wear rate (after 400m sliding) was greatest for specimens plasma nitrided at 550°C (4.550.20), which has the thickest compound layer and a relatively low hardness. On the other hand, total wear rate (after 2000m sliding) is greatest for specimens treated for 1h (1.500.20) which has the lowest hardness and minimum case depth values of all plasma nitrided groups.

Under the test conditions, untreated steel behaved poorly in terms of dry wear resistance due to its low hardness. Worn surfaces of untreated specimens revealed severe running-in wear at the beginning of the test. As a result, metallic wear debris and material loss were observed. The weight loss of untreated specimens increased almost linearly with increasing sliding distance, and always remained higher than those of the plasma nitrided samples.

Severe running-in wear did not occur in the plasma nitrided specimens and wear proceeded in a mild mode throughout the test.

Worn surfaces of untreated and some plasma nitrided samples after a sliding distance of 400m is shown in Fig.4.33. The wear scars formed on the pins are parallel to the rolling direction of the wear rings. Examination of the untreated samples at the early stage of testing revealed extensive wear by adhesion with local fusion, i.e. severe adhesive wear (Fig.4.33a). On the other hand, plasma nitrided samples are seen to be lightly scored with some abrasive particles which are obviously the fragments of compound layers broken at the very outset of the wear test during asperity deformation. Although the worn surfaces had been cleaned with alcohol before SEM study, some fragments of compound layers, which are adhering loosely to the surface and acting as abrasive particles, are clearly visible in Fig.4.33b and c.

SEM micrograph of a plasma nitrided sample after a sliding distance of 1200m is shown in Fig.4.34. The surface is highly scored and the effect of broken compound layer particles is still visible.

Wear surfaces of an untreated and a plasma nitrided samples that had covered, under test, a sliding distance of 2000m are shown in Fig.4.35. A considerable extent of plastic deformation was observed on the wear surface of the untreated specimen (Fig.4.35a). The surface is rough and deeply torn typical of the severe wear. The plasma nitrided sample which exhibited many shallow grooves experienced a reduced degree of damage and plastic deformation on the wear surface (Fig.4.35b). The worn surface of plasma nitrided sample showed typical properties of mild wear with a more oxidized and smooth appearance in comparison with the untreated sample.

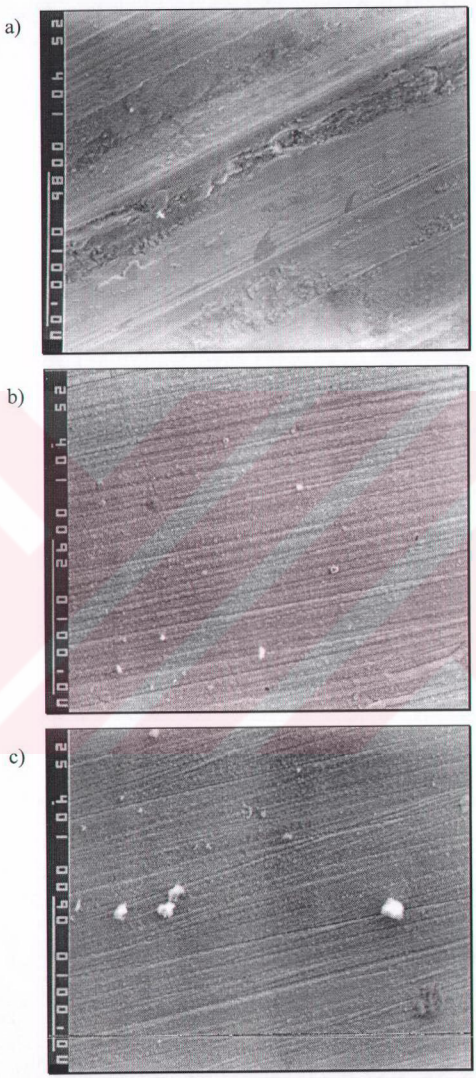

Figure 4.33 Scanning electron micrographs of worn surfaces of some specimens after a sliding distance of 400m a) Untreated b) Nitrided at500°C for 4h (4.500.20) c) Nitrided at 550°C for 4h (4.550.20)

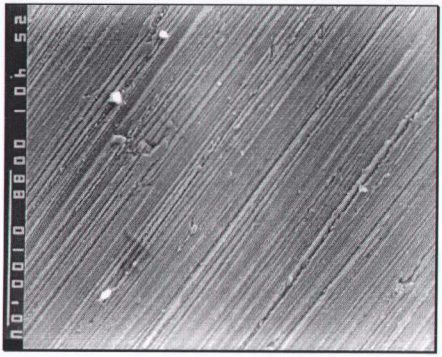

Figure 4.34 Scanning electron micrograph of a 4.550.20 sample showing the worn surface after a sliding distance of 1200m

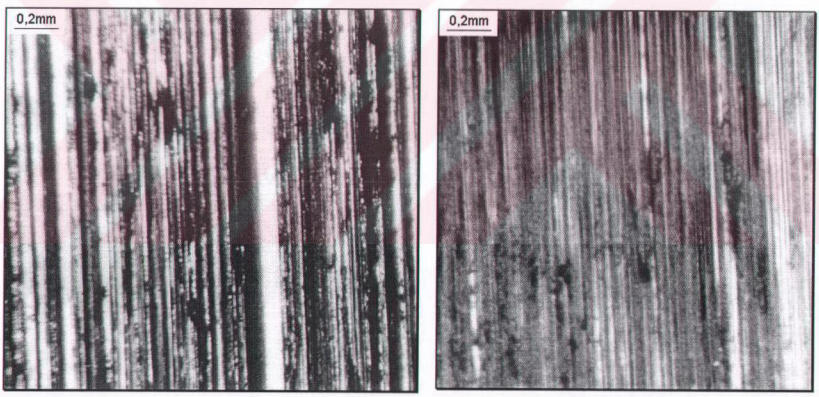

a b

Figure 4.35 Optical micrographs showing wear surfaces of a) untreated and b) plasma nitrided (4.500.20) samples after a sliding distance of 2000m

Optical microscopy examinations show that the worn surface and debris morphology are in close relationship with the wear mechanism. Optical micrographs of wear debris of some specimens are given in Fig.4.36. Large and predominantly metallic debris of untreated sample (Fig.4.36a) shows that, the specimen severely worn under the test conditions. Wear debris produced from nitrided sample was a mixture of plate-like large products of early

periods and very fine brown powders (Fig.4.36b). The oxidized appearance of the worn surface and the generation of oxide wear debris indicate that mild oxidative wear was dominant in the wear of the nitrided samples.

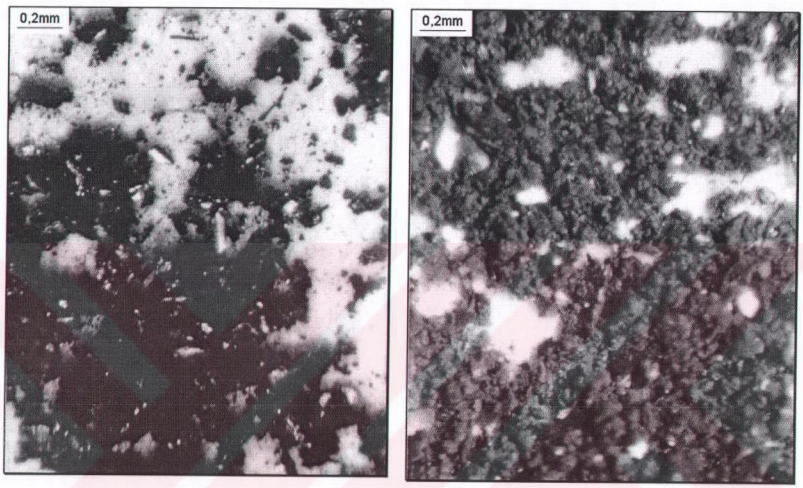

Figure 4.36 Morphology of the wear debris particles produced from pins of a) Untreated and b) Plasma nitrided (4.500.20) samples

The higher weight loss of sample 4.550.20 especially at the first stage of the test (see Fig.4.32) seems to be an effect of its relatively thick compound layer (11μm) and low hardness (See Table 4.1). Here, thicker compound layer increases the wear rate of the sample by breaking off and by forming abrasive particles. This detrimental effect of excessive compound layer thickness was felt especially on specimens having a very thick compound layer like 4.550.20 samples. The particles generated from breakdown of the thicker compound layers change the wear mechanism from adhesive to abrasive. Thus the wear rate is increased with increasing compound layer thickness.

There is very little difference among the wear rates of samples within the first 400m of dry sliding, except 4.550.20 samples. The weight loss values of samples differs with increasing sliding distance. Thus, properties of the nitrided layers, i.e. plasma nitriding

parameters affect the wear resistance of the samples. Higher values of process temperature, which leads thicker compound layer and lower surface hardness, and sorter process times leading to lower hardness values, seems to be the main causes of low wear resistance observed on samples 4.550.20 and 1.500.20.

It can be seen that the weight loss increased with test time (see Fig.4.32). The hardness of the surface is the most effective factor with respect to wear rate. Under the same conditions, the minimum weight loss is observed on the samples treated at 500°C for 4 h due to its high hardness value, i.e. 986HV (see Fig.4.6). The reason for the rapid weight loss of samples treated at 550°C is also related to its relatively low hardness of the case which is not strong enough to support the thick and brittle compound layer.

When the material loss is compared on the basis of the test results, it is found that the combination of high hardness, thin compound layer and thick case is better in reducing the extent of material loss under the test conditions.

CHAPTER FIVE
CONCLUSIONS

5.1 CONCLUSIONS

The main conclusions obtained in this study about effects of plasma nitriding process parameters on mechanical and structural characteristics of AISI 5140 steel, are summarized as follows:

- The outermost layers or compound layers of all samples consisted of a mixture of γ′-nitride and ε-nitride phases. A pure nitride phase (γ′ or ε) has not been observed on the samples produced under the plasma nitriding conditions used here.
- A gradual transformation from ε-nitride to γ′-nitride occurs with increasing treatment time, increasing process temperature and decreasing nitrogen content of the plasma nitriding atmosphere.
- γ′-nitride forms at greater depths than ε-nitride

- Hardness level, case depth, and compound layer thickness are strongly affected by the **process time**.
- With regard to the process time, the sample plasma nitrided over a period of 4h (at 500°C) produces an optimum nitride precipitate size and density leading to the maximum surface hardness. For the sortest time (1h) the nitrogen uptake and precipitate density are low and therefore the amount of hardening is also low. Over extended nitriding periods, surface hardness of samples decreased due to the coarser precipitates.
- The case depth and compound layer thickness are found to be parabolic with time. Compound layer thickness shows an increasing trend with increasing time, but it

seems to reach a saturation. The saturation may be explained by surface sputtering which causes decarburisation of the surface leading to tranformation of iron-nitrides from ε to γ′. This transformation has a limiting effect on compound layer thickness.

- The **process temperature** has a strong influence on both case depth and compound layer thickness. Case depth and compound layer thickness increase greatly with increasing treatment temperature due to an increased rate of nitrogen diffusion.
- At low temperatures (450°C), since the mobility of substitutional solutes is low, a growth limited situation prevails and leads to a low precipitate density and a consequent lower hardness of the layer. Higher nitriding temperatures (550°C) correspond to higher mobilities of the substitutional solutes, but here a nucleation limited situation prevails. Therefore the precipitates are larger, again resulting in lower hardness.

- There does not seem to be any obvious correlation between **N_2 content** of the gas mixture and surface hardness levels. The case depths are similar for all the ratios of N_2 to H_2, but seems to slightly decrease as the amount of N_2 increases. On the other hand, an increase in N_2 gas content of the plasma nitriding atmosphere increases the compound layer thickness.

- Surface modification of the low alloy steel via plasma nitriding substantially improves the **fatigue** behaviour of the steel. The degree of improvement is dependent upon the structural characteristics of the component.
- It is clear that, fatigue strength of the steel increases with increasing process time and temperature obviously due to the increasing case depth.
- All the specimens exhibited a similar fatigue behavior irrespective of the nitrogen content of plasma atmosphere. Slightly lower fatigue strength of specimens treated in an atmosphere with high nitrogen concentration (60% N_2) may be related to their slightly lower surface hardness.
- Fatigue strength of a plasma nitrided sample is determined by its hardness and case depths rather than its compound layer.
- Fatigue fractography investigation of plasma nitrided specimens revealed subsurface

crack initiation especially at stresses corresponding to long lives. The reason for the nucleation of the cracks below the surface is obviously the strengthening of the surface material and generation of the compressive residual stresses on the surface.

- It is evident that the **wear** resistance of the steel is increased markedly by plasma nitriding. The degree of improvement depends on the plasma nitriding process conditions
- The maximum improvement was achieved for the specimens plasma nitrided at 500°C for 4 hours due to its high hardness value. Thus, the hardness of the surface is a very important factor with respect to wear rate
- Thick and brittle mixed-phase compound layer produced on the samples treated at high temperatures (550°C) is extremely brittle and increases the wear rate of the material. The particles generated from breakdown of the thick compound layers at the outset of the wear tests change the wear mechanism from adhesive to abrasive. Thus the wear rate is increased with increasing compound layer thickness and excessive compound layer thickness may be considered to be a defect.
- Higher values of process temperature, which leads thicker compound layer and lower surface hardness, and shorter process times leading to lower hardness values, have been determined as the main causes of relatively low wear resistance of some samples.
- When the material loss is compared on the basis of the test results, it is found that the combination of high hardness, thin compound layer and thick case is better in reducing the extent of material loss under the test conditions.

REFERENCES

Albarran, J.L., Juarez-Islas, J.A., & Martimez, L. (1992). Nitride width and microhardness in H-12 ion nitrided steel. Materials Letters, 15, 68-72.

American Society for Testing and Materials. (1982). a) E 466-76 and b) E 739-80. Annual Book of ASTM Standards, part 10. Philadelphia.

Bell, T., & Sun, Y. (1990). Load bearing capacity of plasma nitrided steel under rolling-sliding contact. Surface Engineering, 6 (2), 133-139.

Berghaus, B. (1932). Process for the surface treatment of metal pieces (German). German patent DRP 668.639.

Berghaus, B. (1939). Vacuum furnace heated by a glow discharge (German).German patent DRP851.540.

Berghaus, B. (1956). Control of glow discharge processes. US patent 3.018.409.

Berghaus, B. (1961). Method and apparatus for controlling glow discharge processes. US patent3.345.280.

Chyou, S.D., & Shih, H.C. (1990). Structure and electrochemical properties of plasma-nitrided low alloy steel. Materials Science and Engineering, A129, 109-117.

Cohen, A., Boas, M., & Rosen, A. (1986). The influence of ion nitriding parameters on the hardness layer of 15-5 ph stainless steel. Thin Solid Films, 141, 53-58.

Collins, J.A. (1981).Failure of Materials in Mechanical Design p.369 John Wiley & Sons.

Çelik, A., & Karadeniz, S. (1995). Improvement of the fatigue strength of AISI 4140 steel by an ion-nitriding process. Surface & Coatings Technology, 72, 169-173.

Çelik, A., & Karadeniz, S. (1996). Investigation of the compound layer formed during ion nitriding of AISI 4140 steel. Surface & Coatings Technology, 80, 283-286.

Edenhofer, B. (1974 a). Physical and metallurgical aspects of ionitriding-part1. Heat Treatment of Metals, 1, 23-28

Edenhofer, B. (1974 b). Physical and metallurgical aspects of ionitriding-part2. Heat Treatment of Metals, 2, 59-67.

Edenhofer, B. (1976). The ionitriding process-thermochemical treatment of steel and cast iron materials. The Metallurgist and Materials Tecnologist, 8, 421-426.

Haruman, E., Bell, T., & Sun, Y. (1992). Compound layer characteristics resulting from plasma nitrocarburising in atmospheres containing carbon dioxide gas additions. Surface Engineering, 8 (no:4), 275-282.

Hombeck, F., & Bell, T. (1991). Environmentally harmless plasma thermochemical processes. Surface Engineering, 7 (1). 45-52.

Hudis, M. (1973). Study of ion-nitriding. Journal of Applied Physics, 44, 1489-1496.

İnal, O.T., & Robino, C.V. (1982). Structural characterisation of some ion-nitrided steels. Thin Solid Films, 95, 195-207.

Jones, J.K., & Martin, S.W. (1964). Brazing Glow Discharge. Metal Progress, 85, 95-98.

Jones, B.K., & Martin, J.W. (1977). Residual stress distribution in nitrided En 41B steel as function of case depth. Metals Technology, 4, 520-523.

Jones, B.K., & Martin, J.W. (1978). Fatigue failure mechanisms in a nitrided En 41B steel. Metals Technology, 5, 217-221.

Karamış, M.B. (1991). Friction and wear behavior of plasma nitrided layers on 3% Cr-Mo steel. Thin Solid Films, 203, 49-60.

Karamış, M.B. (1992). Some effects of the plasma nitriding process on layer properties. Thin Solid Films, 217, 38-47.

Karamış, M.B. (1993). Wear properties of steel plasma nitrided at high temperatures. Materials Science and Engineering, A168, 49-53.

Kovacs, W., & Russelll, W. (1986). Proc. Int. Conf. on Ion Nitriding. T. Spalvins (Ed.), An introduction to ion nitriding. (pp. 9-16). ASM International.

Kölbel, J. (1965). The formation of nitride layers in glow discharge nitriding. (German). Report 1555, Forschung Bericht Lande Nordrhein-Westfalen.

Kuppusami, P., Sundararaman, D., & Raghunathan, V.S. (1993). Comparative study of plasma nitriding behavior of a type 316 stainless steel and a microalloyed steel. Surface Engineering, 9 (2). 137-141.

Kurny, A.S.W., Mallya, R.M. & Mohan Rao, M. (1986). A study on the nature of the compound layer formed during the ion nitriding of En40B steel. Materials Science and Engineering, 78, 95-100.

Kurny, A.S.W., Mallya, R.M., & Mohan Rao, M. (1988). On the formation of austenite during ion-nitriding of armco iron. Journal of the Less-Common Metals, 144, 201-207.

Lampe, T., Eisenberg, S., & Laudien, G. (1993). Compound layer formation during plasma nitriding and plasma nitrocarburising. Surface Engineering, 9 (1), 69-76.

Li, S., Manory, R.R. (1996). Surface morphology and compound layer pores of plasma nitrocarburised low carbon steel. Metallurgical and Materials Transsactions A, 27A, 135-143.

Michalski, J. (1993). Ion nitriding of Armco iron in various glow discharge regions. Surface and Coatings Technology, 59, 321-324.

Miller, K.J. (1993). Materials science perspective of metal fatigue resistance. Materials Science and Technology, 9, 453-462.

Miyamura, H., Takada,J., Kuwahara,H., & Kikuchi, S. (1986). Ion-nitriding behaviour of Fe-Ti alloys in the α-phase region. Journal of Materials Science, 21, 2514-2518.

Özbaysal, K., İnal, O.T., & Romig, A.D. (1986). Ion-nitriding behaviou of several tool steels. . Materials Science and Engineering, 78, 179-191.

Peng, Q.F. (1989). Improving abrasion wear by surface treatment. Wear, 129, 195-203.

Phillips, V.A., & Seybolt, A.U. (1968). A Transmission electron microscopic study of some ion-nitrided binary iron alloys and steels. Transactions of the Metalurgical Society of AIME, 242, 2415-2422.

Rembges, W. (1986). Proc. Int. Conf. on Ion Nitriding. T. Spalvins (Ed.), Fundamentals applications and economical considerations of plasma nitriding. (pp. 189-198). ASM International.

Robino, C.V. & İnal, O.T. (1983). Ion nitriding behavior of several low alloy steels. Materials Science and Engineering, 59, 79-90.

Sato, K., Takahashi, K., Inoue, Y., Yamazaki, T., & Nitoh, Y. (1988). Surface layers produced by ion nitriding of austenitic Fe-Mn-Al alloys and the effects on hardness and corrosion resistance. Journal of Materials Science, 23, 4445-4449.

Seybolt, A.U. (1969). Some observations on the metallurgy of ion-nitriding. Transactions of the Metalurgical Society of AIME, 245, 769-778.

Sun, Y., & Bell, T. (1991). Plasma surface engineering of low alloy steel. Materials Science and Engineering, A140, 419-434.

Sun, Y., Bell, T., & Wood, G. (1994). Wear behavior of plasma nitrided martensitic stainless steel. Wear, 178, 131-138.

Takada, J., Ohizumi, Y., Miyamura, H., Kuwahara, H.,Kikuchi, S., & Tamura, I. (1986). Ion-nitriding of an Fe-19wt% Cr alloy. Journal of Materials Science, 21, 2493-2496.

Tibbetts, G.G. (1974). Role of nitrogen atoms in ion-nitriding. Journal of Applied Physics, 45, 5072-5073.

Xu, X., Wang, L., Yu, Z., & Hei, Z. (1996). Transmission electron microscopy study on the cross-sectional microstructure of an ion-nitriding layer. Metallurgical and Materials Transsactions A, 27A, 1347-1352.

Zlatanovic, M., Kunosic, A., & Tomcik, B. (1986). Proc. Int. Conf. on Ion Nitriding. T. Spalvins (Ed.), New development in adode plasma nitriding. (pp. 47-51). ASM International.

APPENDIX

The application of the bi-linear curve fitting to the fatigue test results of 4.500.20 specimens:

SLOPE PART OF S-N CURVE

According to ASTM E739 (ASTM,1982), the slope part of S-N curve and the standard deviation of fatigue lives can be calculated by the following equations:

Here, the symbol "caret" (^) denotes estimate (estimator), the symbol overbar (¯) denotes average and k is the number of .specimens used for the slope part (k=12 for our study).

$$\boxed{\log N = \hat{A} + \hat{B} \cdot S}$$

$$\hat{A} = \overline{\log N} - \hat{B} \cdot \overline{S}$$

$$\hat{B} = \frac{\sum_{i=1}^{k} (S_i - \overline{S}) \cdot (\log N_i - \overline{\log N})}{\sum_{i=1}^{k} (S_i - \overline{S})^2}$$

$$\overline{\log N} = \frac{1}{k} \sum_{i=1}^{k} \log N_i$$

$$\overline{S} = \frac{1}{k} \sum_{i=1}^{k} S_i$$

The estimated standard deviation of the logarithmic fatigue life σ(logN) is

$$\hat{\sigma}(\log N) = \left[\frac{1}{k-2} \sum_{i=1}^{k} \left\{ \log Ni - (\hat{A} + \hat{B} \cdot Si) \right\}^2 \right]^{1/2}$$

The estimated standard deviation of the fatigue strength σ(S) is

$$\hat{\sigma}(S) = \frac{1}{|B|} \hat{\sigma}(\log N)$$

First 12 specimens (see Table 4.4) which belong to finite fatigue life region were used for the slope part of the S-N curve. Data table and sample calculation are given below:

number	N_i	S_i	S_i-S	$(S_i-S)^2$	$\log N_i$	$\log N_i$-logN	$(S_i-S)x(\log N_i-\log N)$	↓ $(S_i-S)x(\log N_i-\log N)$
1	48600	700	43,75	1914,06	4,69	-0,35	-15,31	0,000062
2	52400	700	43,75	1914,06	4,72	-0,32	-13,88	0,001647
3	65700	675	18,75	351,56	4,82	-0,22	-4,11	0,004312
4	79800	675	18,75	351,56	4,90	-0,13	-2,52	0,000353
5	91400	675	18,75	351,56	4,96	-0,08	-1,42	0,006040
6	86500	650	-6,25	39,06	4,94	-0,10	0,62	0,022708
7	98600	650	-6,25	39,06	4,99	-0,04	0,27	0,008804
8	133400	650	-6,25	39,06	5,13	0,09	-0,55	0,001402
9	142300	625	-31,25	976,56	5,15	0,12	-3,64	0,019316
10	171800	625	-31,25	976,56	5,24	0,20	-6,20	0,003268
11	235700	625	-31,25	976,56	5,37	0,34	-10,49	0,006428
12	343500	625	-31,25	976,56	5,54	0,50	-15,60	0,059410
		656,25		8906,25	5,04		-72,8457	0,13375
		S		SUM1	logN		SUM2	SUM3

B= SUM2 / SUM1
= -72,8457 / 8906,25 B = -0,0082

A= 5,04 - (-0,082) x 656,25 A= 10,40416

$\log N = 10{,}40416 - 0{,}0082 . S$

$\sigma(\log N) = [\ (1/10) \times 0{,}13375\ ]^{1/2} = 0{,}11565$

$\sigma(s) = (1 / 0{,}082) \times 0{,}11565 = 14{,}10$ Mpa

HORIZANTAL PART OF S-N CURVE

The fatigue tests were carried out in accordance with the sequential nature of the up & down or staircase method. 9 specimens labeled between 4.500.20-13 and 4.500.20-21 were used used for the horizantal part of S-N curve (see Table 4.4).

After the fatigue tests, the data is tabulated as follows: All stress levels experienced by the less frequent event is listed in column I. In column II the number '0' is assigned to the lowest stress level, '1' is assigned to the next higher stress level etc. The number of times the event occurred at each stress level is listed in column III. The product of column II times column III is tabulated in column IV.

The statistical estimate of mean fatigue strength at the prescribed life (here $2x10^6$) is calculated from:

$$\hat{S}_e = S_0 + d\left[\frac{A}{N} \pm \frac{1}{2}\right]$$

where

$\hat{S}e$ = Statistical estimate of mean fatigue strength, MPa
S_0 = Lowest stress level at which the less frequeny event occured
d = step size, MPa
N = total number of less frequent events
A = sum of column IV

The plus sign (+) is used if the less frequent event is runout, and the minus sign (-) is used if the less frequent event is a failure.

Accordingly, the data can be tabulated and estimated fatigue strength can be calculated as follows:

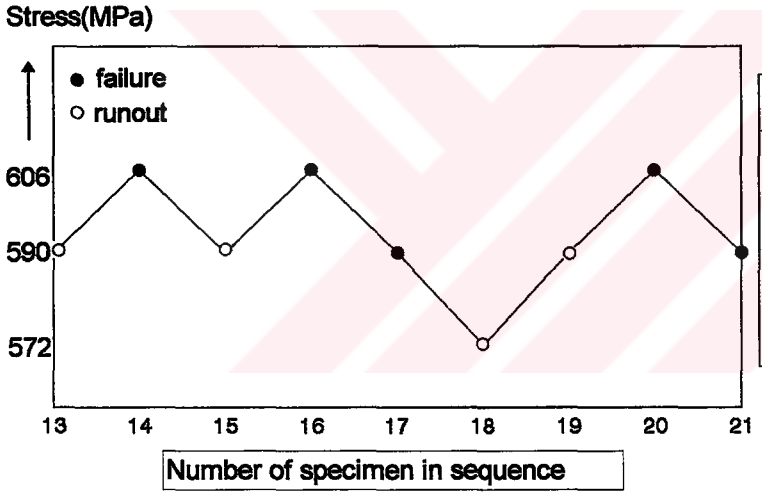

I	II	III	IV
606	2	0	0
590	1	3	3
572	0	1	0
		N=4	A=3

$$\hat{S}e = 572 + 16\left[\frac{3}{4} + \frac{1}{2}\right] \Rightarrow \hat{S}e = 592 \text{ MPa}$$

Stress step, d

(+), because less frequent event is runout in the example

The End